

General Disclaimer

One or more of the Following Statements may affect this Document

- This document has been reproduced from the best copy furnished by the organizational source. It is being released in the interest of making available as much information as possible.
- This document may contain data, which exceeds the sheet parameters. It was furnished in this condition by the organizational source and is the best copy available.
- This document may contain tone-on-tone or color graphs, charts and/or pictures, which have been reproduced in black and white.
- This document is paginated as submitted by the original source.
- Portions of this document are not fully legible due to the historical nature of some of the material. However, it is the best reproduction available from the original submission.

FINAL REPORT

Submitted By

University of Rhode Island
Department of Physics
Kingston, Rhode Island 02881

TITLE: Fiber Optic Pressure Sensors in Skin-Friction Measurements

Robert Kidwell (Graduate Student)

Robert S. Kidwell

Frank W. Cuomo (Advisor)

Frank W. Cuomo

Surendra S. Malik (Physics Dept. Chairman).

S. Malik

(NASA-CR-176294) FIBER OPTIC PRESSURE
SENSORS IN SKIN-FRICTION MEASUREMENTS Final
Report (Rhode Island Univ.) 57 p
HC 104/MF A01

N86-11838

CSCI 06B

G3/52

Unclas
15887

September 1985



FOREWORD

This technical report is respectfully submitted by the Physics Department of the University of Rhode Island to the Electro-Mechanical Instrumentation Branch (Dr. A.J. Zuckerwar), Instrument Research Division, NASA Langley Research Center, Hampton, VA., in fulfillment of the deliverables, mutually agreed upon, pertaining to Grant No. NAG-1-519.

TABLE OF CONTENTS

	<u>Page</u>
FORWARD	
ABSTRACT	
INTRODUCTION.....	1
EXPERIMENTAL METHODS AND RESULTS.....	2
STATUS OF RESEARCH WITH LIQUID CRYSTALS.....	8
SUMMARY.....	8
FUTURE EFFORTS.....	9
FIGURES.....	11
REFERENCES.....	25
#1.....	26
#2.....	31
#3.....	36
#4.....	40
#5.....	48

ABSTRACT

Fiber optic lever pressure sensors intended for use in a low speed wind tunnel environment were designed, constructed and tested for the measurement of normal and shear displacements associated with the pressures acting on a flat aluminum plate. On-site tests performed at LaRC along with several static and dynamic measurements made at the University of Rhode Island have established that, with proper modifications and improvements, the design concepts are acceptable and can be utilized for their intended use.

INTRODUCTION

The intent of this project is to investigate the utilization of a three-fiber optical lever in the design and construction of two pressure sensors of minimal dimensions, one of which is designed for the measurement of shear motion associated with skin-friction, and one for normal pressure measurements. This includes the construction of prototype sensors to be tested in the low velocity wind tunnel at Langley Research Center. The basic concept of a three-fiber lever, which might be used in a sensor of this type, has been analyzed by F.W. Cuomo in Reference 1, which provided the impetus for this research. A fiber bundle consisting of three fibers, one transmit and two receive fibers of unequal core diameters is utilized. The distal end of the bundle is positioned near a reflective element which is displaced by applied pressure (normal or shear), causing modulation of the light signals from the receive fibers. By using the differential output of the unequal receive fibers, considerable improvement in sensitivity is observed.

Our research this year can be broken down into several efforts leading to the design and construction of suitable sensors:

- a. The analytical study to establish the most promising optical fiber core dimensions, the optimum spacing between cores, the fiber arrangement at the distal end and the mirror configuration for the shear and pressure sensors.
- b. The experimental determination of the elastic moduli, the attenuation constants and the linearity at sub-micron motion of optically clear elastomers derived from silicone compounds (See Reference 2).
- c. The design and implementation of suitable electronics to efficiently couple to the photodetectors and generate the output ratio upon which the improved sensitivity is based. The major obstacles to the attainment of acceptable signal detection have been associated with noise and frequency response.

d. The initial phase of experimentation using a three-fiber probe. D.C. measurements were made for both shear and longitudinal or normal pressure cases, and much improvement over previous designs was achieved. Measurements of A.C. response of the probes were made indicating that the probe responses are independent of frequency in the range of interest.

e. Design and construction of pressure and shear pressure sensors using a reflector incorporated in an elastomeric element.

f. Testing of the sensors in the wind tunnel facility at LaRC. Tests focused on the DC and broadband AC response of the sensors to pressure and shear motion in the tunnel.

g. D.C. pressure calibration tests to establish linearity and level of response of the constructed pressure sensors to static pressures somewhat higher than those generated in the low speed wind tunnel.

Central to the shear sensor part described in effort (a) was the development of an analytic model for shear motion, involving reflective stripes or half-planes for the reflective surface, which would be similar to that proposed by Cuomo (Ref. 1) for a full mirror. This shear model is detailed in Ref. 3. The arrangement of fibers which was eventually used in both shear and pressure sensors consisted of three fibers in contact (close-packed) and closely fitted in a metal tube (see Ref. 3, Figure 1). Another arrangement modeled was three fibers in a straight line viewed end-on with the transmit fiber as the center fiber. While this was more straightforward from a conceptual viewpoint, the analytical results were essentially the same as the close-packed or triangular case and practical consideration led to the choice of the close-packed arrangement.

EXPERIMENTAL METHODS AND RESULTS

In order to verify the geometric model and establish calibration criteria for the three-fiber pressure and shear motion sensors, fiber probes were designed and constructed. Several probes were constructed with different fiber core

diameters and fiber arrangements. Early efforts showed that repeatable orientation of the fibers during assembly of the in-line design, with all three fibers in a line viewed end-on, could not be achieved with available equipment and efforts were therefore concentrated on the triangular or close-packed design. To construct the probes, three fibers were stripped of protective buffer, but not cladding, and cemented with Math Associates, Inc. two-component fiber optic epoxy into a short length of stainless steel hypodermic tubing. The end face of the fibers and tube was then polished flat and perpendicular. The fibers leading from the probe were covered with a protective sheath and terminated with Amp Optimate connectors. Some of the probes were constructed for us by General Fiber Optics, Inc. to take advantage of equipment and procedures not available to us.

Testing of the probes consisted of two distinct procedures, a static or DC test and an AC response test. For the DC test, static displacement measurements of a mirror relative to the fiber probe were made using a differential micrometer. Displacements were perpendicular to the fiber end for the longitudinal test, while the edge of the mirror was displaced through the interaction region in a direction parallel to the probe end for shear motion, as detailed in Ref. 3. The receive fiber signals and the calculated sensitivity for shear motion are shown in Figures 5 and 6 of Reference 3, and can be compared with model predictions in Figures 2 and 3 of the same reference. Figures 1 and 2 of this report show similar results for the longitudinal test. All testing of the shear configuration is done at a fixed distance from the mirror to the probe such that when the mirror fully reflects the incident cone of the light, that is, the mirror edge is outside the cone of light, then the receive fibers are fully illuminated. This ensures the largest response to shear motion of the mirror edge. In addition, in practice this maximum in illumination of the fibers is a broad maximum with reference to the mirror to probe distance; hence the shear sensor is insensitive to small changes in longitudinal distance, and only sensitive to shear motion.

Figure 3 is a block diagram of the test apparatus and electronics used for the static tests. Several light sources were considered for the fiber optic system, including incandescent and laser sources. A high power LED, Motorola MFOE1201, was chosen for the best combination of output power and stability. This LED has a peak wavelength of 820 nm. United Detector Technology (UDT) FO-02-400 photodiodes with maximum sensitivity in this range were used for detection. The output of the LED was voltage modulated in a square wave and the output of the photodiode amplifier was filtered through an Ithaco lock-in amplifier set at 1 Hz bandwidth.

Separate readings were made of the large and small receive fiber outputs and the ratio sensitivity calculated from them. From the results of these DC tests, both longitudinal and shear, optimum mirror positions can be chosen for constructing pressure or shear sensors in a region of linear response near the peak of the sensitivity curves.

The second major test using probes is to determine whether the AC response of the sensors depends on frequency in the range of interest, which was initially taken as DC to 10 KHz. The test consisted of attaching a mirror to the head mass of a piezoelectric transducer in such a way as to provide either longitudinal or shear motion relative to a fiber probe which was positioned at a nominal distance (and lateral position in the shear case) determined from the DC sensitivity curves. A 200/200/50 μm probe was used in these tests. For the longitudinal test a probe-mirror distance of 238 μm was chosen, while the shear test was performed at a mirrored distance of 760 μm and a lateral position of 62 μm referenced to the centerline of the transmit fiber. Figure 4 is a block diagram of the test apparatus. The transducer is driven by a B & K 1022 oscillator at 100 volts (RMS). The output of the photodiode amplifier is fed into an Ithaco lock-in amplifier with a 1 Hz bandwidth. The transducer driving frequency is also used as the

reference frequency for the lock-in amplifier. Thus, by varying the oscillator frequency, the range from 20 Hz to 10 KHz (the maximum frequency range of the lock-in) can be scanned with a constant bandwidth.

In order to establish the frequency dependence of the transducer, a commercial piezoelectric accelerometer was mounted in place of the mirror on the transducer face and the output of the accelerometer recorded as a function of frequency. Figure 5 shows the AC response of the large and small receive fiber for the shear configuration, while Figure 6 provides the ratio response. Similarly, Figures 7 and 8 show the longitudinal data. The response of the accelerometer was converted into displacement assuming the relationship $x = \frac{a}{\omega^2}$, where a is the acceleration, x is the displacement and ω is the angular frequency. Figure 9 is the calculated displacement from the accelerometer showing good agreement with the probe data. This indicates no frequency dependence in the probes themselves in this range. Structure common to all of the curves can be assumed to be resonances of the transducer.

A separate experimental study was carried out to determine the elastic moduli and attenuation coefficients of optically clear elastomers. Static measurements of Young's Modulus and dynamic sound speed measurements were performed on several elastomers. In addition tests were performed to evaluate the linear behavior of an elastomeric element within the micron displacement range. These tests are detailed in Ref. 2 and the results tabulated in Table III of Ref. 2. Consideration of this data led to the choice of three Petrarch Systems elastomers for use in constructing the sensors.

Several sensor devices were designed and constructed for testing in the low velocity wind tunnel at LARC. Figures 10 and 11 show the basic design of the pressure and shear sensors. The machining of the brass sensor components was done at the Langley Research Center. The mirrors are 1/8" diameter and .007" thick. The mirrors were manufactured by depositing aluminum with a protective

overcoating of silicon monoxide on a thin glass substrate, which was then scribed and cut to size. Some of the substrates were masked during deposition in order to provide a final mirror which was only silvered on one half of the circular substrate with a straight line demarkation for the shear sensors. Assembly of the sensors in general is as follows: the mirror is suspended in a curved elastomer in the sensor body. The fiber probe is epoxied into the threaded probe holder. Final adjustment of the mirror to probe gap and probe orientation is done by the 6-40 thread probe holder with a lock nut against the body. The body is designed externally to fit a premachined hole in the half-inch aluminum plate in the wind tunnel with a locking nut on the threaded body, as shown in Figures 10 and 11.

Suspending the mirror in elastomers in the sensor body caused some difficulties. The performance of some of the pressure sensors was degraded as a result of elastomer working down in between the mirror surface and the probe. This occurred while filling the region above the mirror. One method of avoiding this is to use a precured material above the mirror. Two additional pressure sensors were assembled in this way at Langley by Sam Harper using poured elastomers below the mirror and silastic foam rubber caps inserted above the mirror. Table 1 lists the elastomers incorporated into sensors which were tested at Langley.

	P1	Pressure P2	P3	P4	Shear SS2	SS3
Below mirror	G.E. RTV 602	G.E. RTV 760	PSW 2061	PSW 2061	-	-
Above mirror	Silastic Foam	Silastic Foam	PSW 2061	PSW 2061	PSW 2061	PSW 2062

TABLE 1. Elastomers Used in Sensors

A summary report of the tests at Langley is attached as ref. 4.

Sheets 1-4 of Ref. 4 show the electronic configuration used in the tests. Graph 2 of Ref. 4 is a summary of the results of the tests, showing the DC and broad-band AC response of the sensors for various air velocities in the wind tunnel.

In addition to performance of the sensors in the low velocity wind tunnel at Langley a static pressure test was performed at the University of Rhode Island to characterize the performance of the sensors at pressures larger than those encountered in the wind tunnel. The factors of interest in this test were the magnitude and linearity of response of the pressure sensors in the higher pressure range up to .36 psi. The report of this test is attached as Ref. 5. Figures 2 and 3 of Ref. 5 show the output change of the two fibers of each sensor, which exhibit the linearity of response which is desirable for operation of the sensors. In addition the pressure sensitivities in psi^{-1} are listed in Table 1 of Ref. 5. For the four sensors tested the table lists both individual fiber sensitivities and the ratio sensitivity, showing a clear improvement in general using the ratio of the two fibers.

For all the testing of the probes and complete sensors, three basic electronic components were used which were constructed by an undergraduate student, Richard Goyette, working under our direction. The light source for the fibers is an LED powered by a circuit which allows either DC operation of the LED or square wave modulation. Figure 12 is a schematic of the LED circuit. For square wave operation an external function generator provides the reference frequency, which is then also supplied as reference to lock-in amplifiers along with the output fiber signals. The light from each receive fiber is detected by a photodiode operated into an operational amplifier with switchable amplifier gain. Figure 13 is a schematic of the photodiode circuit. The amplified output of the photodiode circuit can either be filtered through a lock-in amplifier and the resulting

signals from the two fibers combined in a ratio output using a digital device such as the digital oscilloscope at the Langley wind tunnel facility, or the ratio can be taken using an analog divider circuit. Figure 14 is a schematic of the circuit which was built using an Analog Devices AD538 divider.

STATUS OF RESEARCH WITH LIQUID CRYSTALS

From previous discussions with our sponsor we proposed to investigate the use of liquid crystals in the design of a shear sensor. We have made preliminary observations using liquid crystals to enhance the sensitivity of the detector. As a first attempt we placed a small amount of nematic liquid crystal between two parallel, circular glass plates separated by optical fibers with a cladding diameter of 125 μm . The two glass pieces were treated with lecithin in order to align the molecules perpendicular to the surfaces. One glass was attached to a rigid mount and the other was cemented to a PZT shear transducer. A He-Ne laser beam and crossed polarizers monitored the orientation of the nematic molecules. When an AC voltage was applied to the transducer, the attached glass underwent transverse oscillations which disturbed nematic orientation. We observed an optical response when the applied frequency was in the range 600-2000 Hz for this system. The received signal decreased with increasing frequency.

These preliminary observations were made to show the effect and are predicted by the dynamic theory of liquid crystals. We are now in the process of building thinner cells mounted in elastomer that can be driven by an air flow. The extent to which liquid crystals can enhance the sensitivity is the main goal of the investigation.

SUMMARY

Several criteria are important in the performance of the fiber-optic ratio sensors. From the computer modelling and the experimental data, it can be seen that utilizing the ratio of two unequal fibers gives considerable improvement in sensitivity over individual fiber pairs, one transmit and one receive. The

minimum detectable motion, and hence the smallest detectable pressure change, and the sensitivity are improved by the use of larger fibers to collect more signal, and larger ratios of receive fiber core sizes. The higher pressure static tests shows that the sensors constructed to date perform as expected when larger pressures are measured, although the combination of lower sensor response and higher electronic noise resulted in only very marginal performance in the low velocity wind tunnel.

Several elastomers have been investigated for use in these sensors and techniques developed for incorporating them into the sensors. In addition design and assembly techniques for probes and complete sensors have been developed, resulting in prototype sensors which do perform generally as expected, although with much less response.

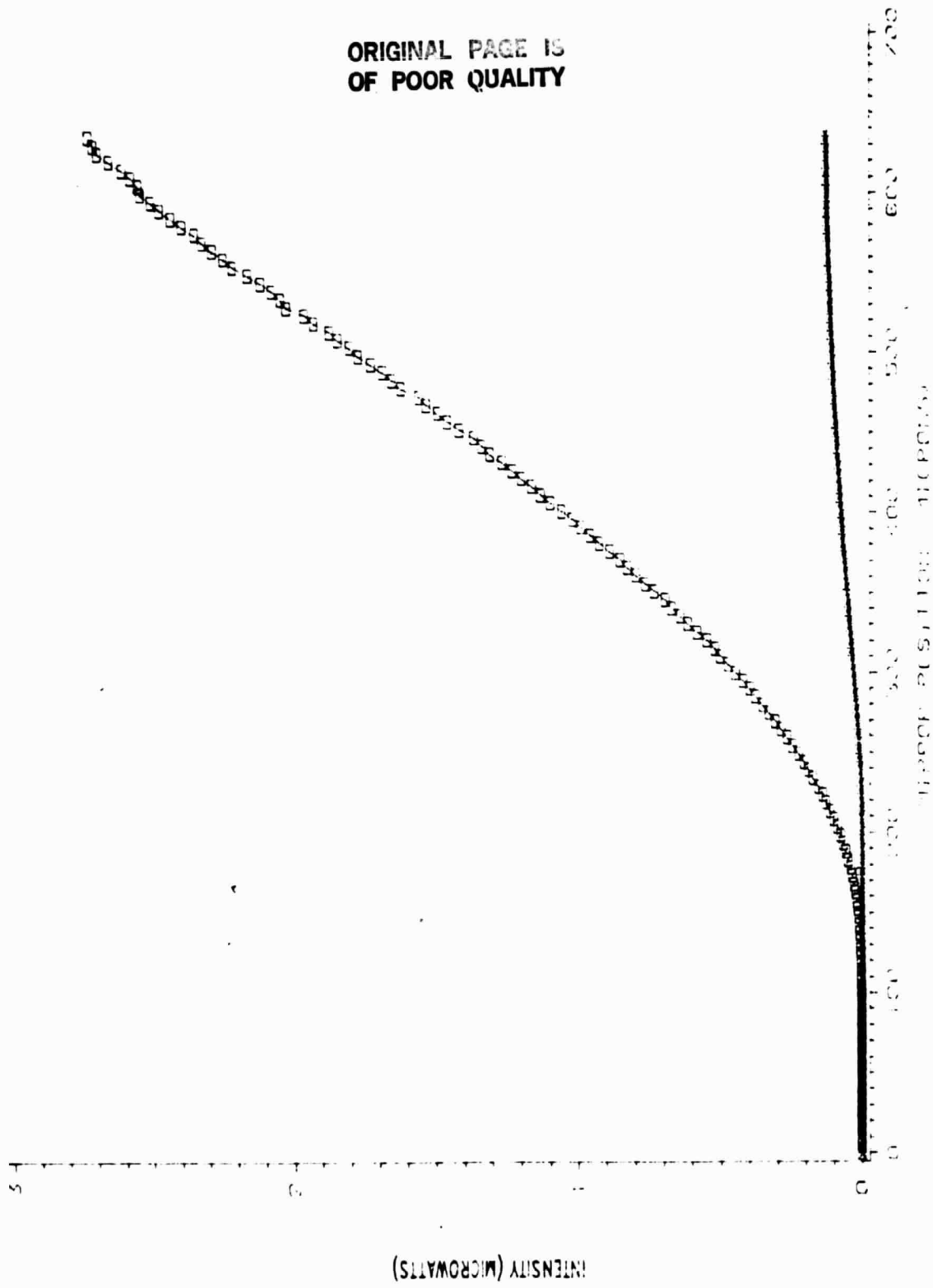
FUTURE EFFORTS

The following action items have been agreed upon by LaRC and URI to improve the sensitivity of the pressure and shear probes:

1. The area of the fibers will be increased, either through increased diameter or greater number of fibers. This will necessitate redimensioning and re-machining the probes. The machining will be done at LaRC.
2. A specification will be added concerning the centerlines of the hole and threads of the fiber probe holder. These should be parallel to within 1/2 deg. for required fiber alignment. The fit of the thread will be changed for class 3 to class 2, if necessary.
3. The elastomer will be changed to one having a lower modulus of elasticity. A possible candidate is RTF760.
4. The design of a schlieren shear probe will be considered.
5. Positive efforts will be made to reduce the electrical noise in the supporting electronics. A zero DC offset will be incorporated into the photodiode amplifier circuit.

6. The length of the probes will be redimensioned to fit the 7"x11" tunnel along the entire test section.
7. Procedures and apparatus will be developed for calibration of both pressure and shear sensors.

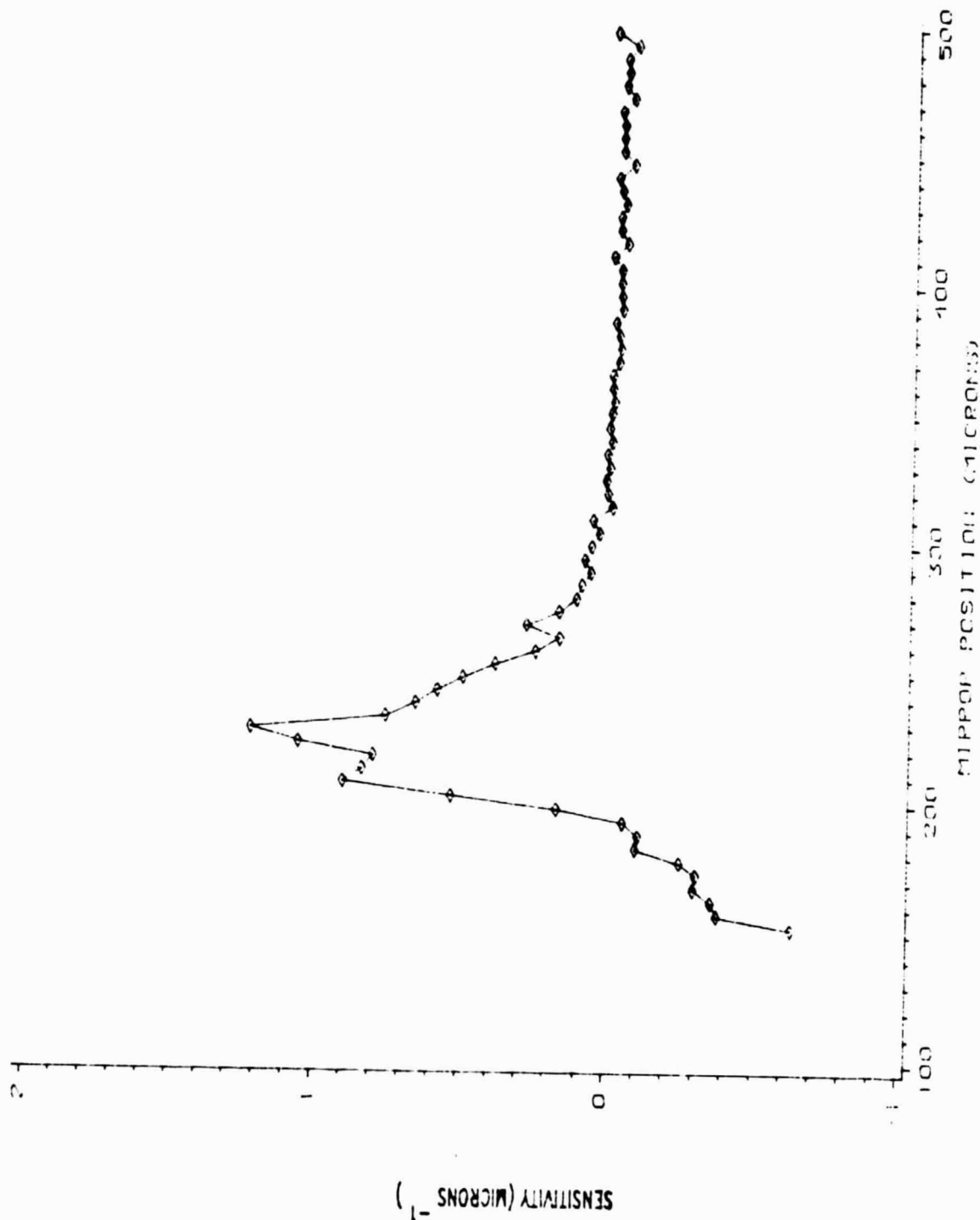
ORIGINAL PAGE IS
OF POOR QUALITY



LONGITUDINAL DATA 200/200/50

FIGURE 1

ORIGINAL PAGE IS
OF POOR QUALITY



LONGITUDINAL DATA 200/200/50

FIGURE 2

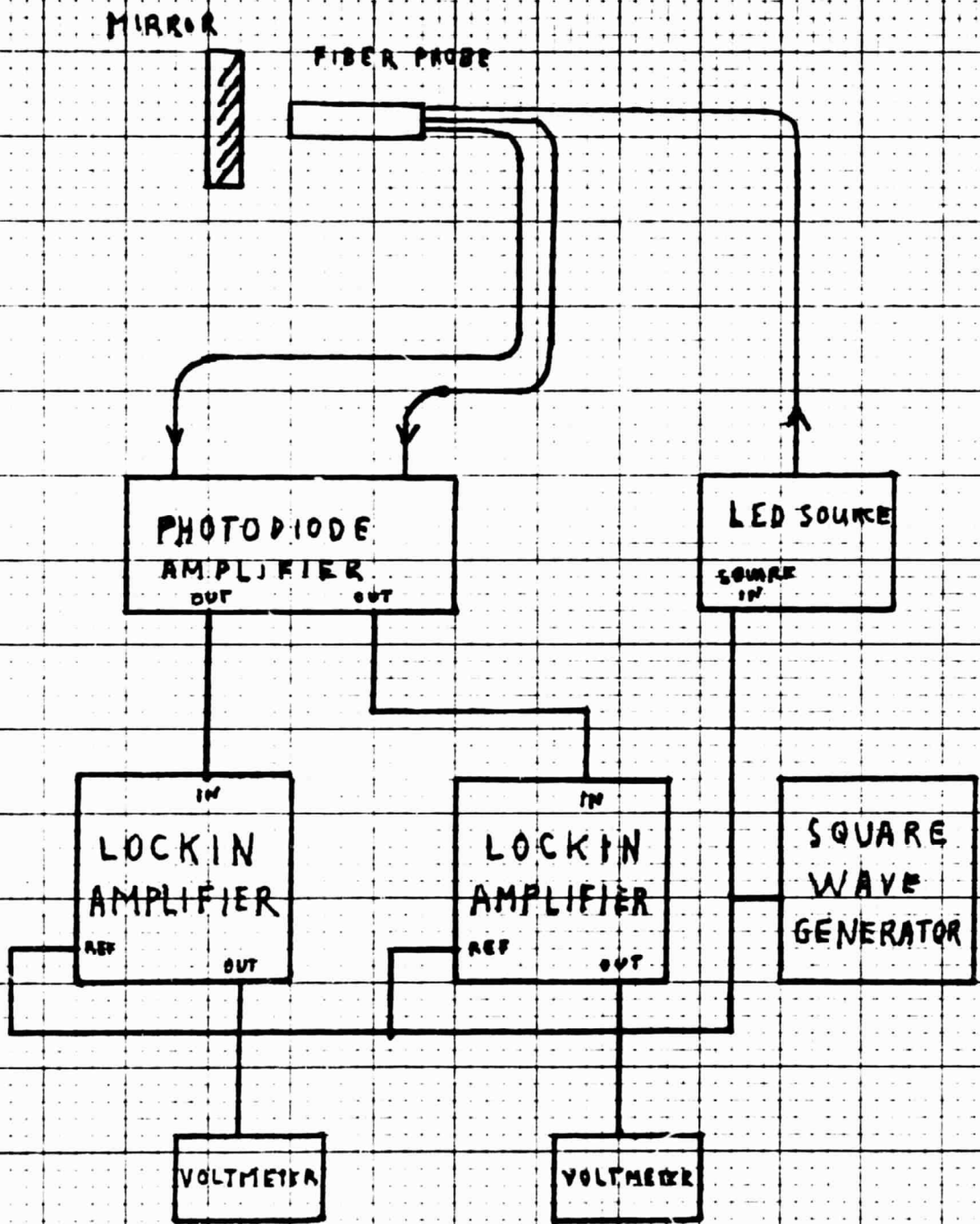


FIGURE 3
DC TEST APPARATUS

ORIGINAL PAGE IS
OF POOR QUALITY

TRANSDUCER

FIBER PROBE

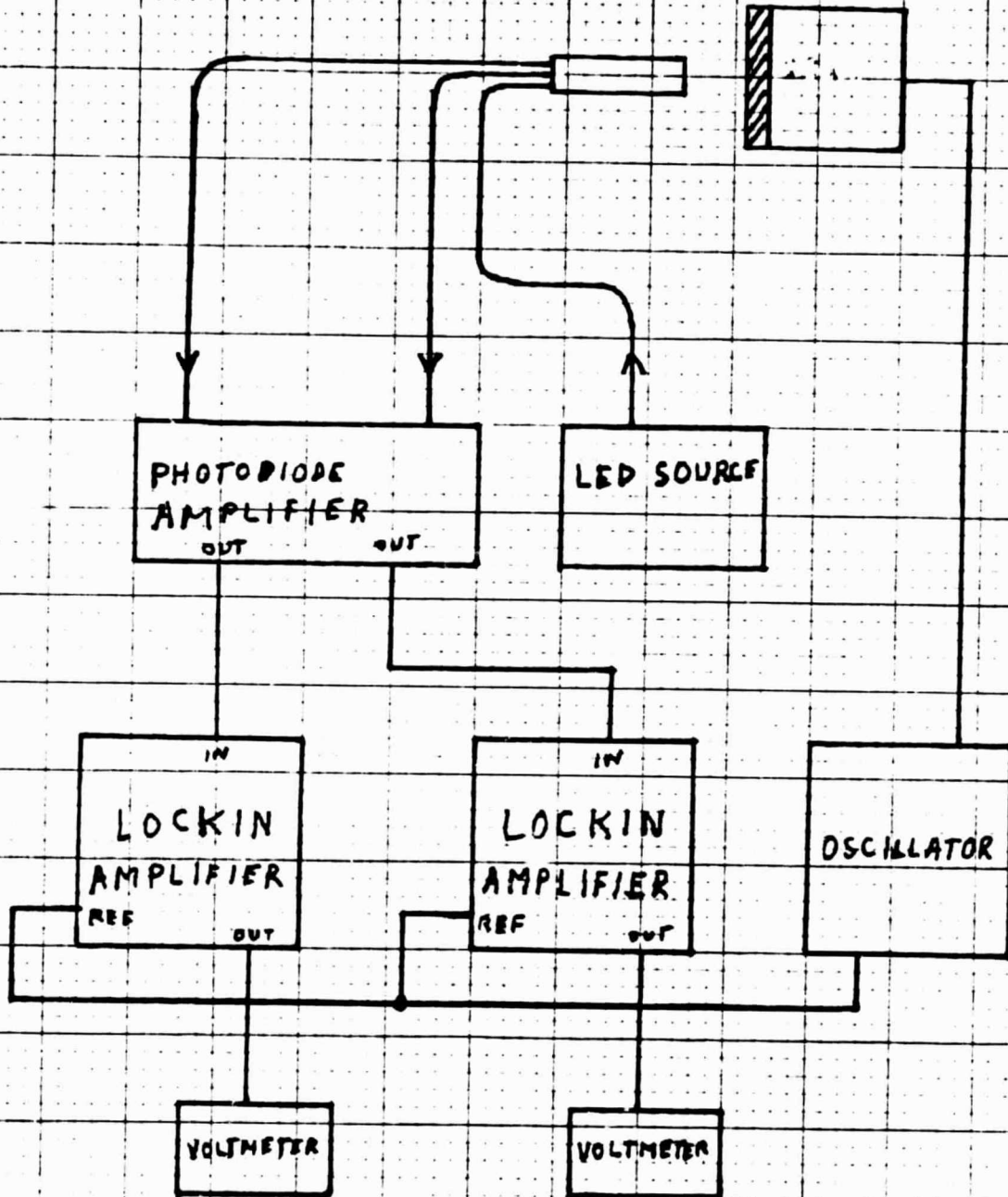


FIGURE 4
AC TEST APPARATUS

ORIGINAL PAGE IS
OF POOR QUALITY

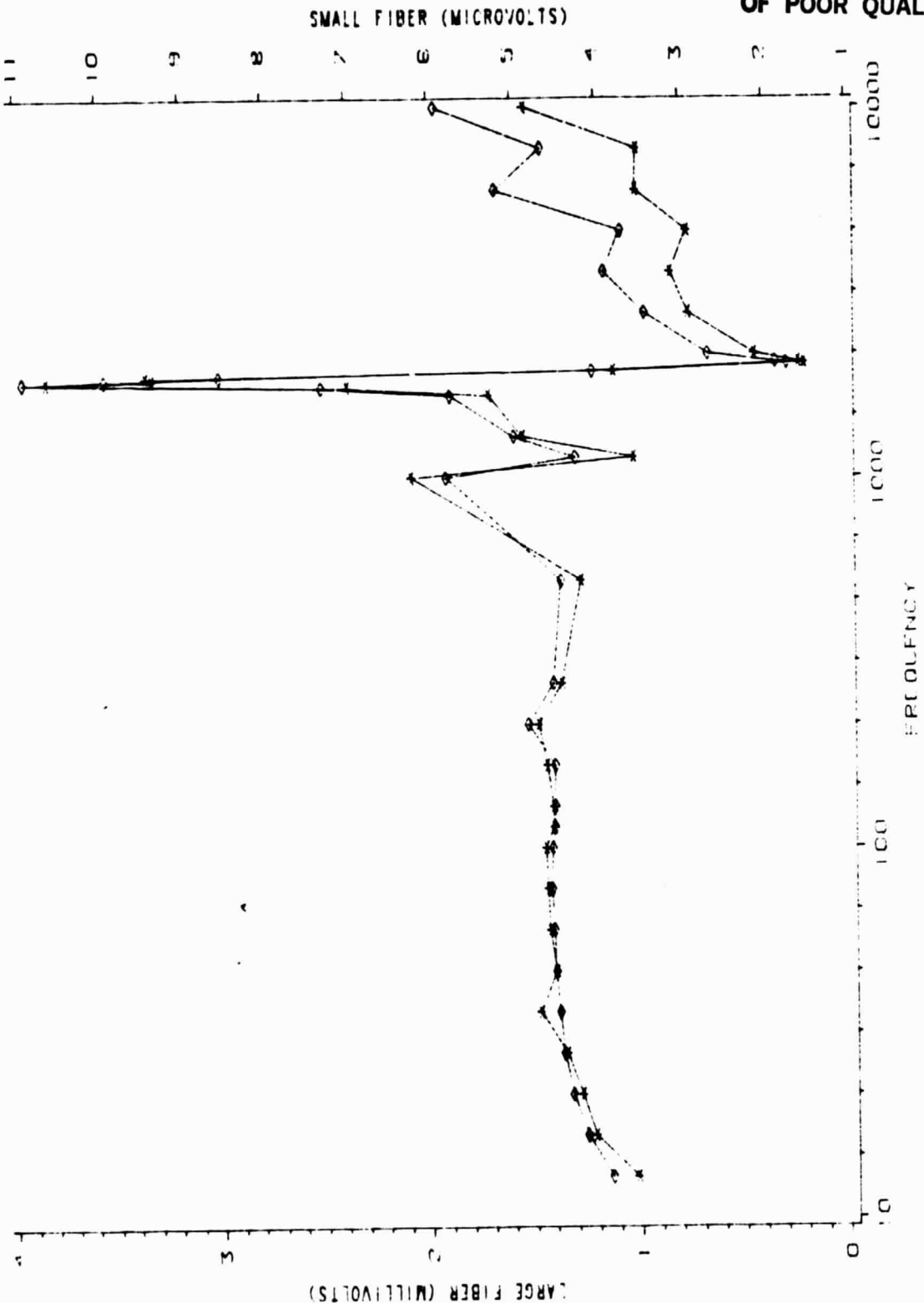
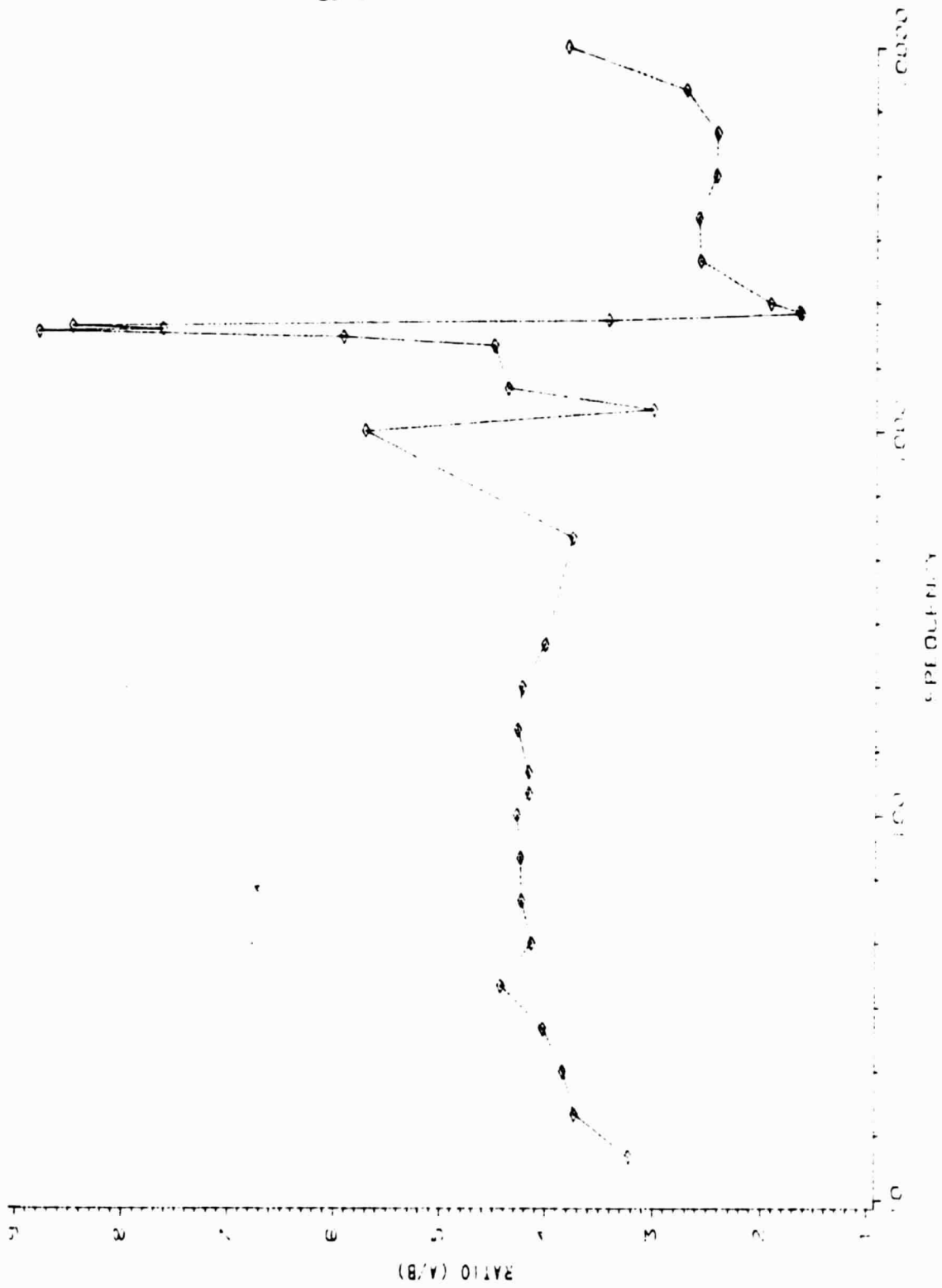


FIGURE 5

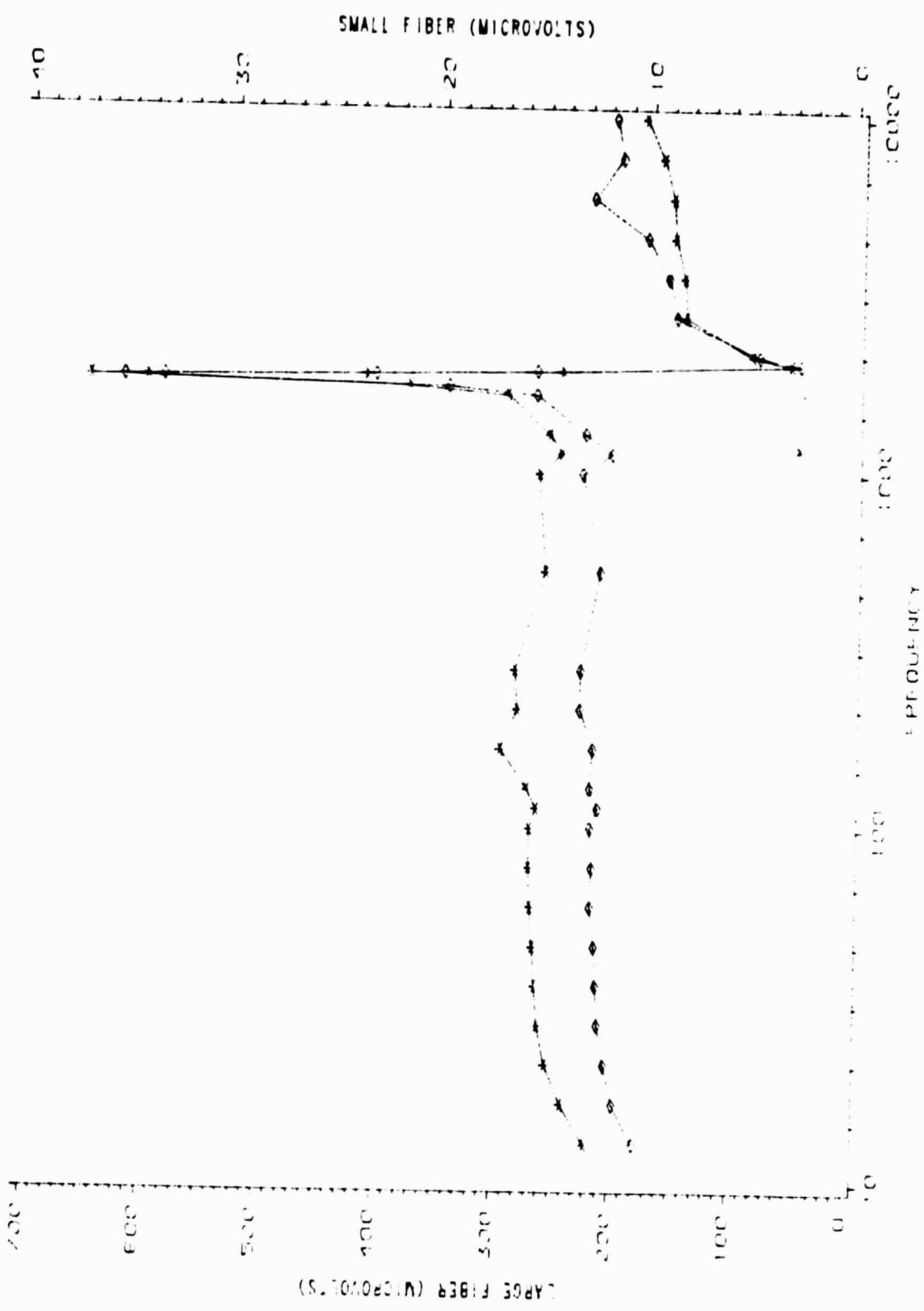
ORIGINAL PAGE IS
OF POOR QUALITY



SHEAR AC

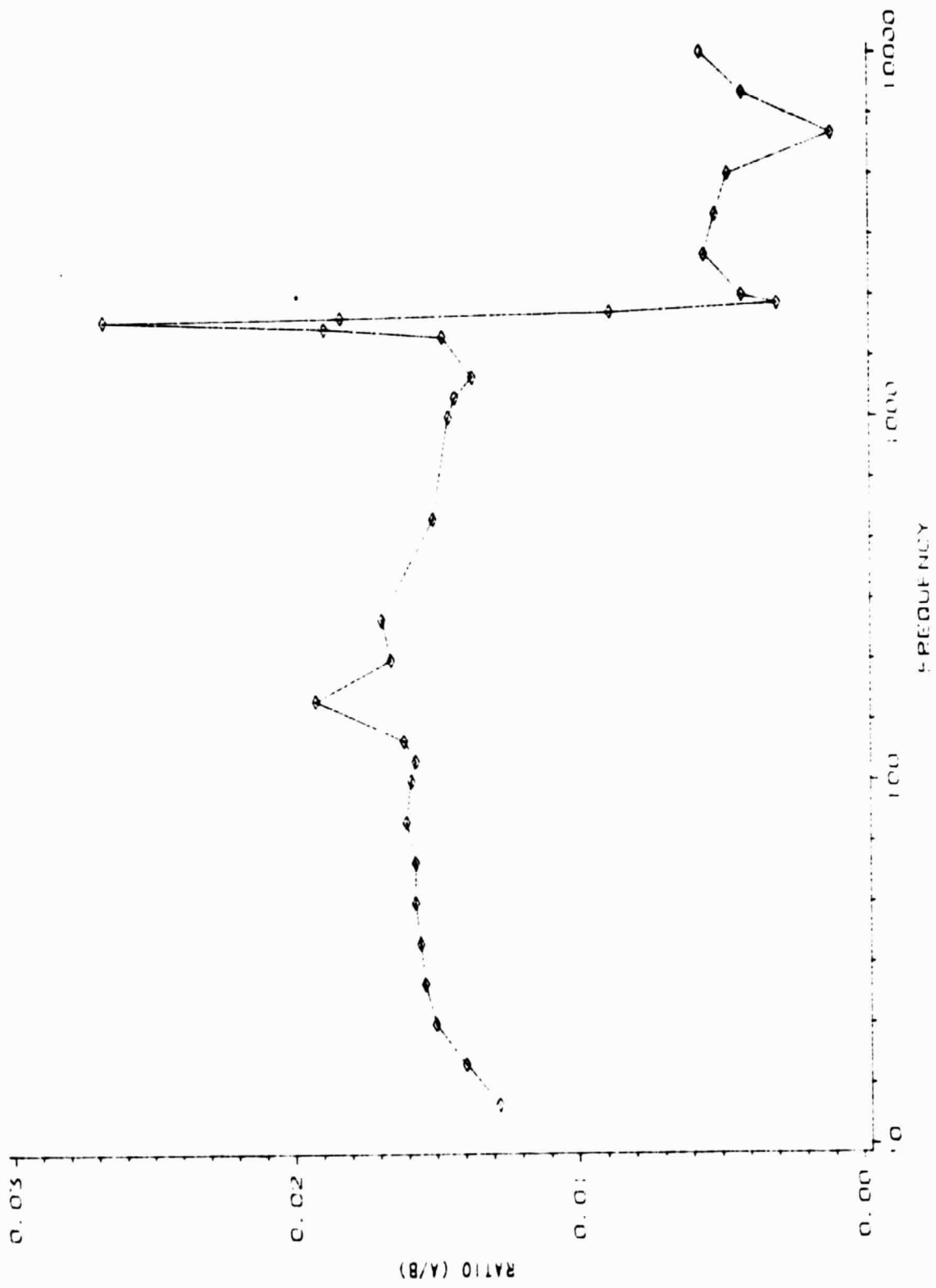
FIGURE 6

ORIGINAL PAGE IS
OF POOR QUALITY



LONGITUDINAL AC
SMALL FIBER (MICROVOLTS)
LARGE FIBER (MICROMETERS)

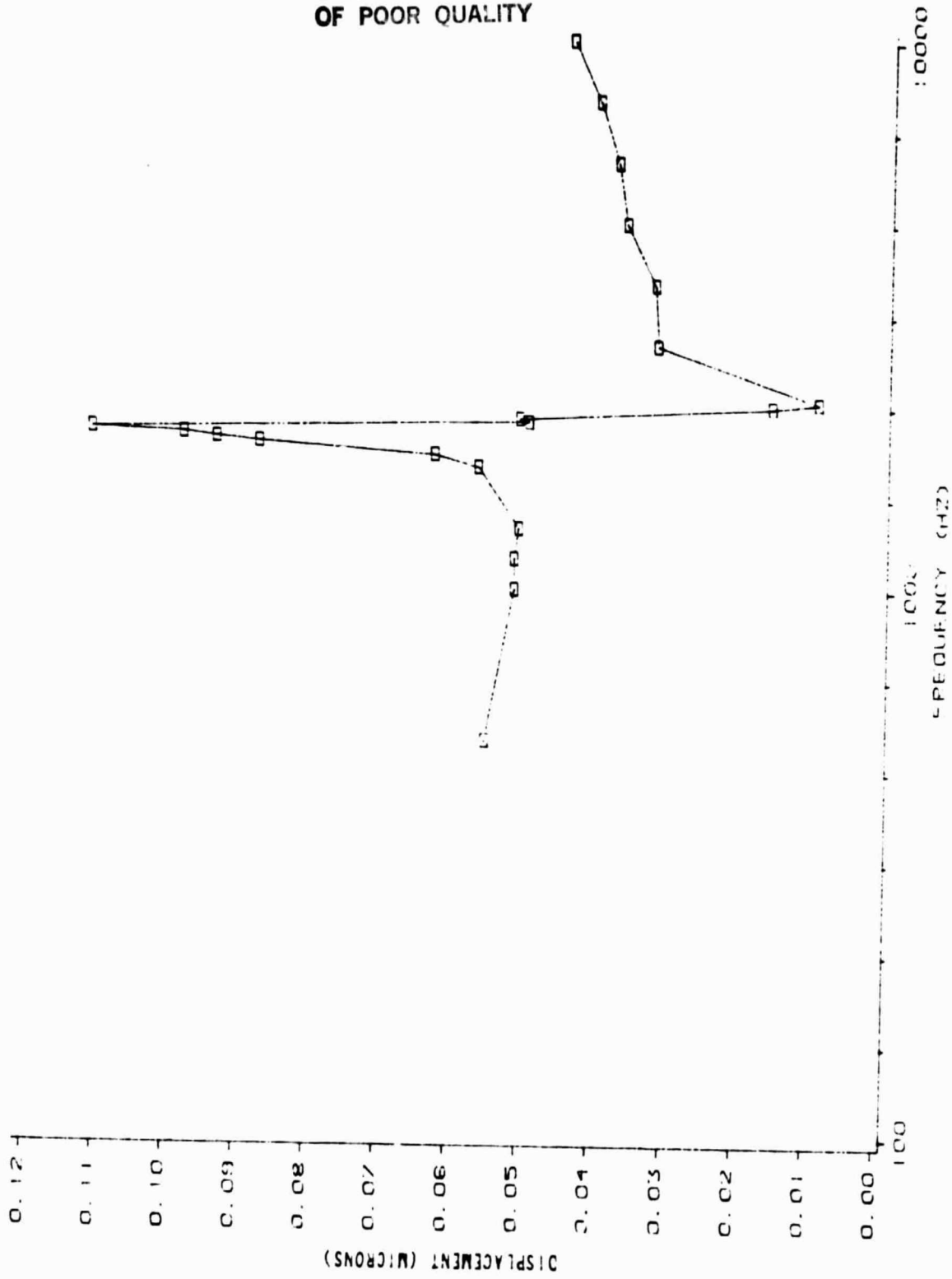
FIGURE 7



LONGITUDINAL AC

FIGURE 8

ORIGINAL PAGE IS
OF POOR QUALITY

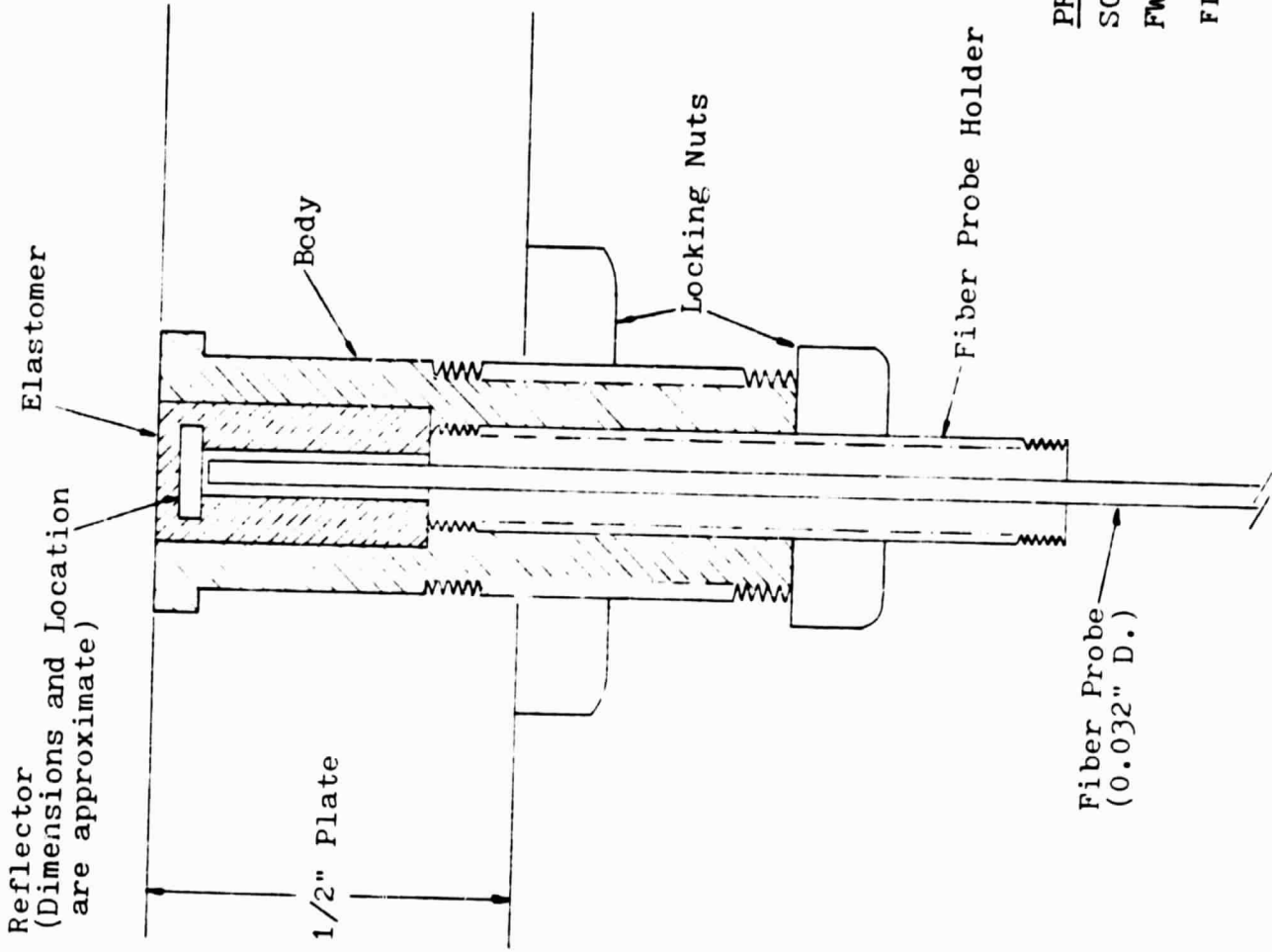


ACCELEROMETER

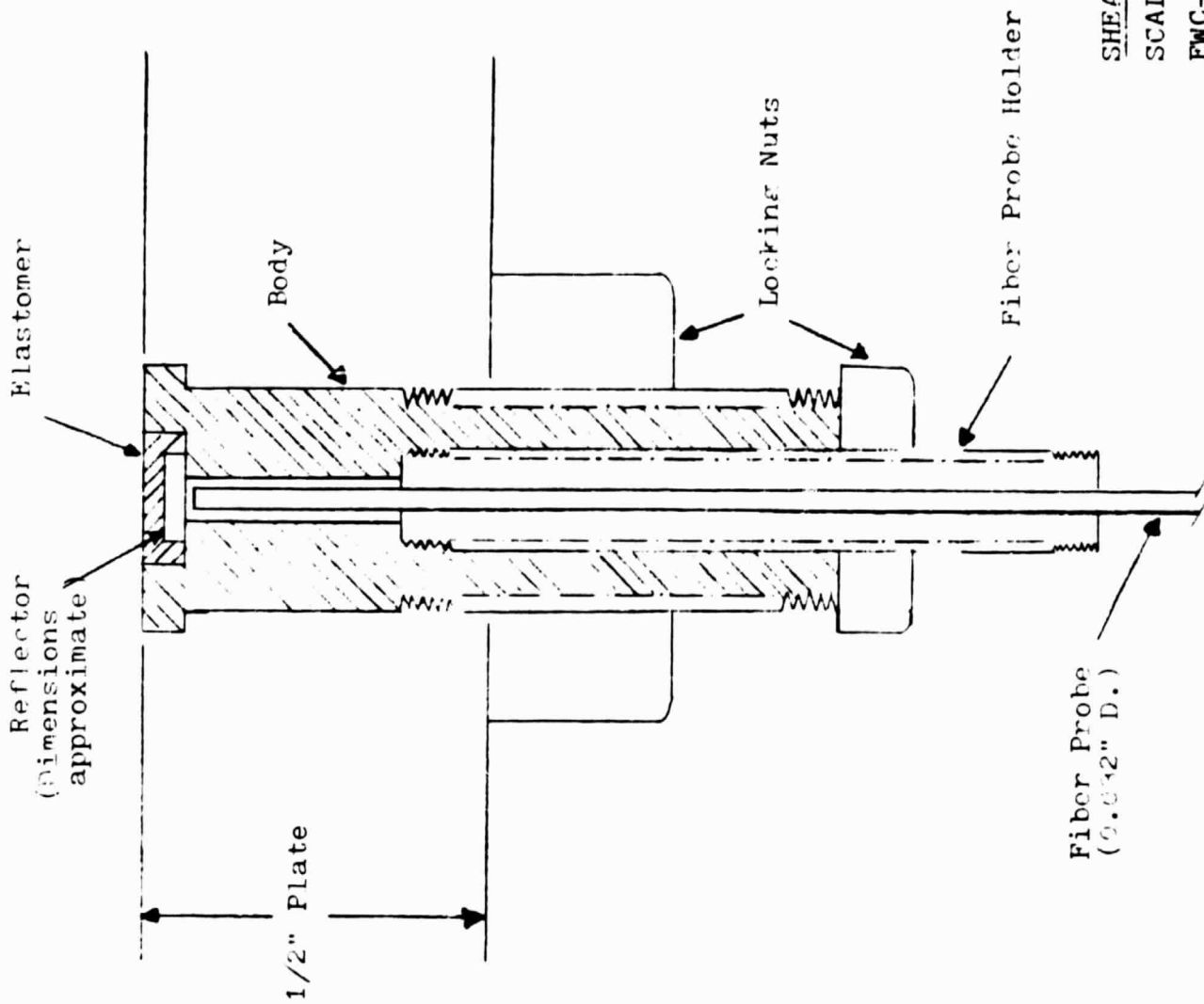
FIGURE 9

ORIGINAL PAGE IS
OF POOR QUALITY

PRESSURE SENSOR
SCALE- 4X
FWC / 5-24-85
FIGURE 10



ORIGINAL PAGE IS
OF POOR QUALITY



SHEAR STRESS SENSOR

SCALE - 4X

FWC-RSK / 5-30-85

FIGURE 11

LED TRANSMITTER CIRCUIT

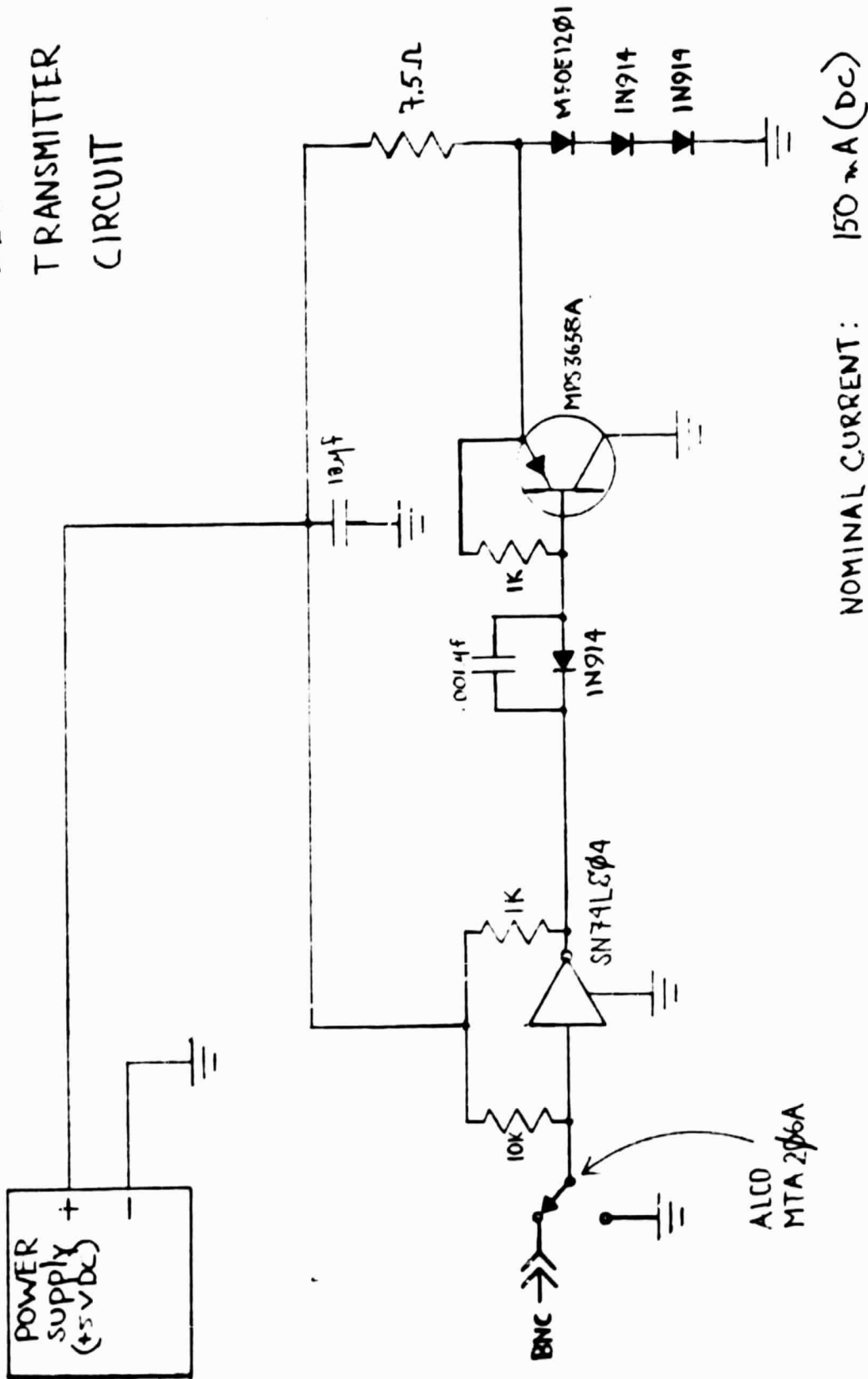
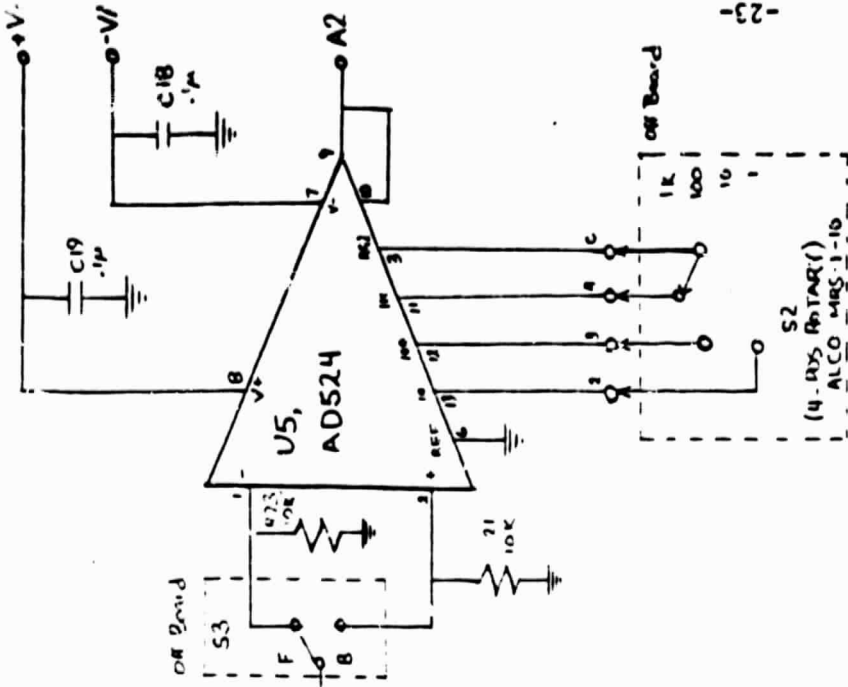
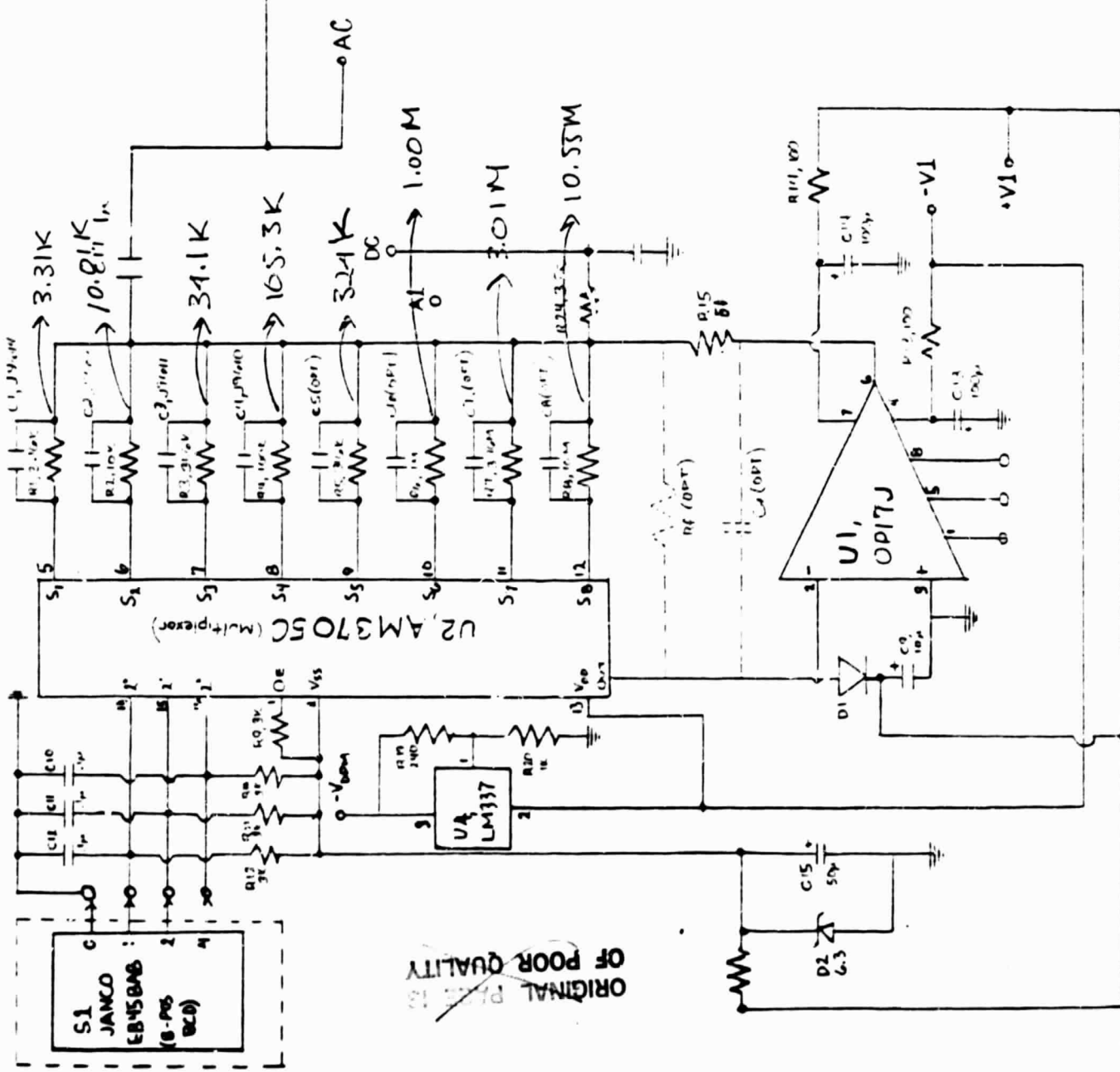
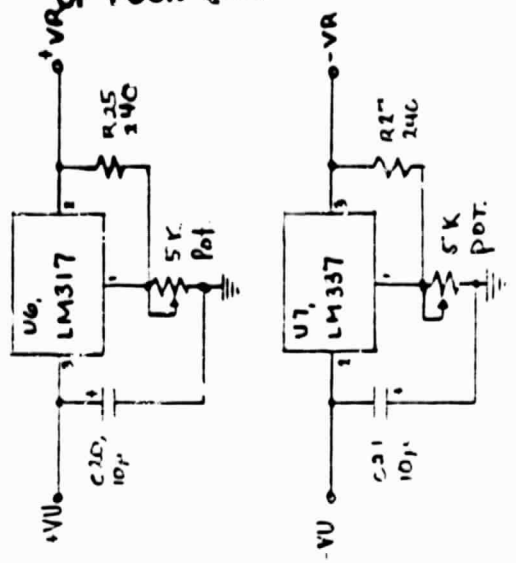


FIGURE 12



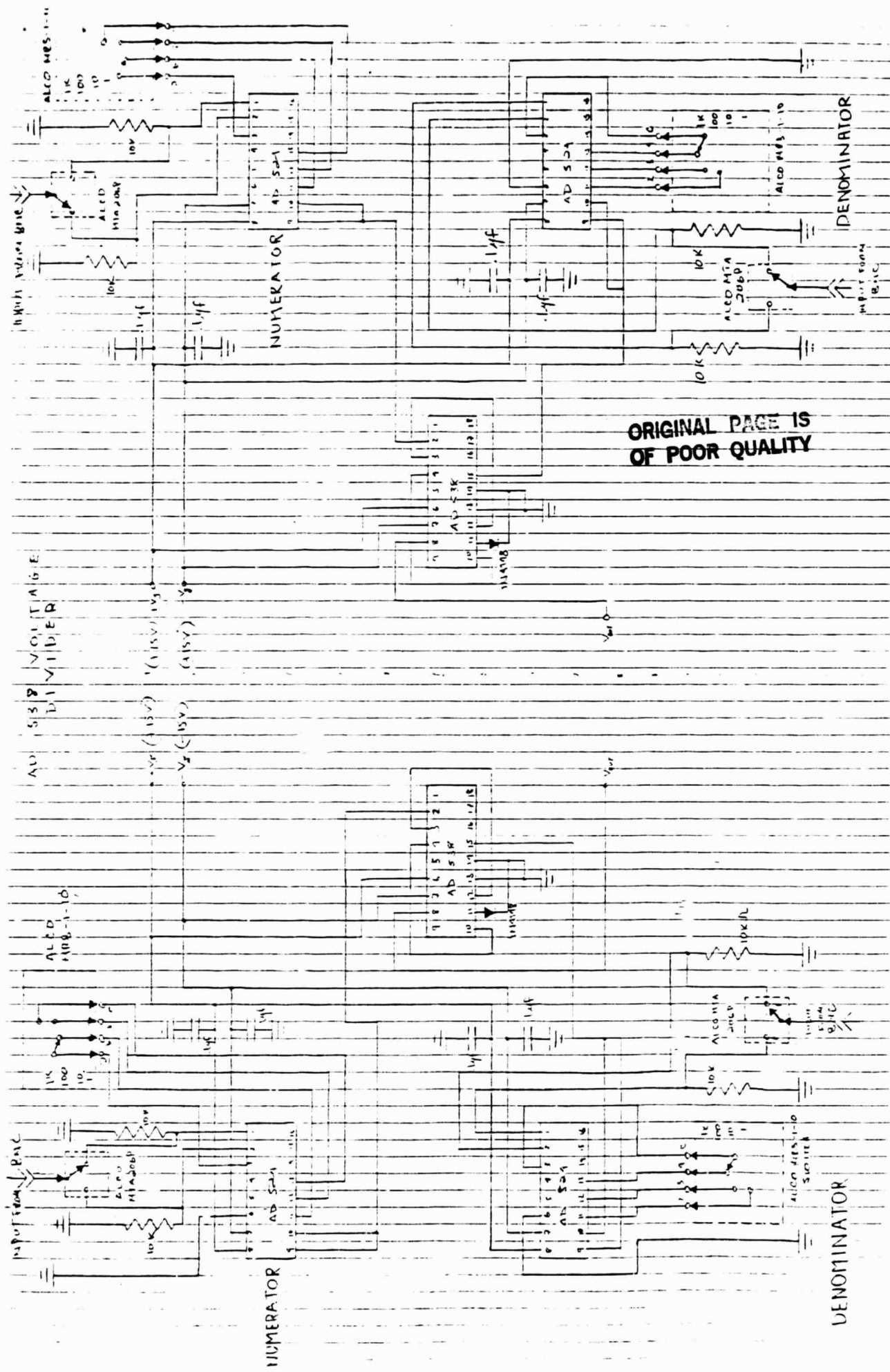
-23-

ORIGINAL PAGE IS OF POOR QUALITY



ORIGINAL PAGE IS OF POOR QUALITY

FIGURE 13 PHOTODIODE AMPLIFIER



ORIGINAL PAGE IS
OF POOR QUALITY

FIGURE 14
AD538 DIVIDER

REFERENCES

1. Cuomo, F.W., "The Analysis of a Three-Fiber Lever Transducer," Proc. SPIE Symposium East, 4/8, 28-32 (1984).
2. Cuomo, F.W., "An Optically Clear Silicone Resin as an Acoustic Element for Fiber Optic Lever Displacement Sensors", Proc. Ultrasonics International 85, London, England (July 1985). To be published.
3. Kidwell, R.S. and Cuomo, F.W., "A Fiber Optic Lever Sensitive to Shear Stress," submitted for presentation at IOOC-ECOC '85 Conference, Venice, Italy (October 1985).
4. Cuomo, F.W., Summary report I (Langley Research Center Wind Tunnel Experiment (August 1985).
5. Kidwell, R.W., Summary Report II (Static Pressure Test) (August 1985).

The analysis of a three-fiber lever transducer

Frank W. Cuomo

Department of Physics, University of Rhode Island, Kingston, R.I. 02881
and
Naval Underwater Systems Center, Newport, R.I. 02841

Abstract

A fiber optic lever sensing technique utilizing three fibers, one transmit and two receive with different core diameters, is described. The method predicts improved sensitivity, and in some cases, larger fiber-reflector gaps than three fibers of equal cores and numerical apertures. Other features include the already established advantages of compensation for input power variations and input fiber losses. It is found that optical fibers with unequal core-cladding diameters as well as numerical apertures provide the most improved results.

Introduction

Non-contacting fiber optic levers have been recently described for several applications. For example, Kobayashi et al.¹ have used them as intracardiac pressure transducers, Cook et al.² have applied them to shock measurements, Cuomo³ has developed pressure and pressure gradient hydrophones while Lawson and Tekippe⁴ have designed a fiber optic sensor determining pressure from the diaphragm curvature. In particular, Reference 4 describes how the diaphragm deflection is derived from the ratio of the light intensity received by two sets of fibers, arranged concentrically with the illumination fibers, at some distance from the diaphragm. It is also indicated that this method compensates for input power variations, fiber losses and changes in reflectivity while the approach used assumes that the core radii of the transmit and receive fibers are identical. This paper utilizes a similar method whereby a three-fiber arrangement consisting of one transmit and two adjacent receive fibers of unequal core diameters is used such that the light reflected from a diaphragm, flat or curved, and collected by the two receive fibers can be processed by means of ratio measurements of the two outputs. The sensitivity of the device can be predicted from the determination of the illuminated portions of the receive fiber cores at any fiber-reflector gap within the useful range of the device.

Theory

The bifurcated two-fiber optic lever has been described in Reference 1, as shown in Figure 1. The light transfer coefficient, η , defines the ratio of the total radiated power from the proximal tip of the receiving fiber to the total incident light power into a transmit fiber. Of the two factors in this equation, the first one represents the light transmission loss while the second is associated with the reflector displacement, as indicated elsewhere.³ In addition, the transducer sensitivity becomes proportional to the coefficient η and the total number of transmit/receive fibers used, while increasing with input/output fiber configurations approaching those shown in Figures 2a and 2b. It is, however, possible to utilize geometrical optics to obtain an approximation to device sensitivity without reference to optical fiber losses, propagation and reflectivity losses or other related parameters. Figure 3 shows the cross-section at the distal end of two adjacent 100 micron fiber cores, one transmit and one receive, and their corresponding areas of illumination projected at the distal end upon reflection. This figure also shows how the illuminated area of the receive fiber, $A_1 + A_2$, can be readily obtained. Since the irradiance is defined as the radiant flux per unit area, one can write

$$P_A / P_0 = A / S \quad (1)$$

where P_A and P_0 are the radiant flux, in watts, at the plane of Figure 3, for the transmit beam and receiving fiber, while S and $A_1 + A_2 = A$ are the corresponding areas of illumination, respectively. A small axial displacement, dq , of the reflector leads to a small change in A/S such that the system sensitivity becomes

$$d(A/S) / dq \quad (2)$$

A similar argument can be used if two receiving fibers adjacent to the transmit fiber are considered, as shown in Figure 4. It is not necessary that the three fibers be collinear. If the two receive fibers have unequal cores, such as 50 and 100 microns, then it is possible to process the outputs A and B of Figure 4. If the radiant flux intercepted by the two receive fibers is P_A and P_B then utilizing Eq. (1) and taking the ratio one obtains

$$(A/S) / (B/S) = A/B \quad (3)$$

where A and B are the illuminated areas of the 100 micron and 50 micron receive fibers, respectively. It is noted that by taking the ratio the quantity S is eliminated from the resulting expression. The ratio sensitivity simply becomes

$$d(A/B) / dq \quad (4)$$

Conversely, the difference divided by the sum of areas A and B can be obtained yielding

$$(A/S - B/S) / (A/S + B/S) = (A-B) / (A+B) \quad (5)$$

and

$$d(A-B/A+B) / dq \quad (6)$$

This approach lends itself to the determination of the optimum arrangement relative to the transmit/receive fiber core dimensions, the distance between fiber core centers and the numerical apertures associated with each fiber. In addition, the index of refraction of the gap medium can be included in the calculations. The following section illustrates to some extent these considerations.

Analytical Results

Computer-generated data are presented based on the theoretical predictions previously described. Figures 5 and 6 show the illuminated area of the receive fiber and the sensitivity of the two-fiber coupling of Figure 1 as a function of the fiber-reflector gap. It is noted that the 100/100 micron fiber pair yields a better sensitivity than the 100/50 micron pair. The numerical aperture was assumed to be 0.25 for all fibers. Figures 7 and 8 provide results for the sensitivities predicted by the ratio as well as the difference over the sum ratio of the three-fiber arrangement of Figure 4. Here, while the gap range is similar to that of Figure 6, best results are predicted for operation near 90 microns as compared to about 5 microns for the two-fiber pair. In addition, the sensitivities show a sizable improvement particularly for the A/B ratio. In order to establish criteria related to fiber core spacing and numerical aperture two commercially available optical waveguides (Corguide) were chosen for evaluation. The transmit fiber used 105/140 core-cladding dimensions with a 0.3 NA while one of the two receive fibers used 52/125 core-cladding and 0.21 NA. The cladding was assumed to remain as part of each fiber. Figures 9 and 10 give the results of the A/B ratio. Figure 10 reproduces a portion of Figure 9 with an expanded sensitivity scale. Several improvements are noted over the previous data. A remarkable increase in sensitivity is observed while the fiber-reflector gap is extended further. Table 1 below summarizes the results presented.

Table 1.

Transmit/Receive Fibers	Output Ratio	Sensitivity (microns ⁻²)	Fiber/Reflector Gap (microns)
100 / 100 0.25 / 0.25 2-Fiber	Core NA	1.10x10 ⁻³	3.87
100 / 100 / 50 0.25 / 0.25 / 0.25 3-Fiber	A/B	1.59x10 ⁻²	93.0
	A-B/A+B	4.37x10 ⁻³	93.0
105-140/105-140/52-125 Core-Cladding	A/B	7.99	135.4
0.30 / 0.30 / 0.21 3-Fiber	A/B	1.40	145.1

Comments

The analytical technique described has been confined to the use of three fibers, one transmit and two receive with different cores and numerical apertures. It should be obvious that larger sensitivities can be realized with a greater number of fibers. For example, the arrangement shown in Figure 2c can be used with the six output fibers consisting equally of two dissimilar core-cladding diameters. This increase can be obtained without a dimensional change of the transducer. It is noted that, with the potential for better sensitivities per number of fibers used, much smaller devices can be built for acoustic detection, flow measurements and medical applications. Although experimental work on this project is well underway, pertinent data is not available at this time and will be made available at a later date.

Conclusions

It is found that geometrical optics, utilizing the illuminated areas approach, can be effectively applied to predict the sensitivity and fiber-reflector gap operating range of fiber optic lever sensors. The advantages of this technique include the ability to generate near optimum conditions related to fiber core and cladding dimensions, spacing between core centers and numerical apertures.

References

1. Kobayashi, K., Okuyama, H., Kato, T., and Yasuda, T., "Fiberoptic Catheter-Tip Micro-manometer," J. J. Med. Electron. Biol. Eng., Vol. 15, pp. 25-32. 1977.
2. Cook, R., O., Hamm, C., W., and Akay, A., "Shock Measurement with Non-Contacting Fiber Optic Levers," J. Sound Vib., Vol. 76, pp. 443-456. 1981.
3. Cuomo, F., W., "Pressure and Pressure Gradient Fiber-Optic Lever Hydrophones," J. Acoust. Soc. Am., Vol. 73, pp. 1848-1857. 1983.
4. Lawson, C., and Tekippe, V., J., "Fiber-Optic Diaphragm-Curvature Pressure Transducer," Opt. Lett., Vol. 8, pp. 286-288. 1983.

ORIGINAL PAGE IS
OF POOR QUALITY

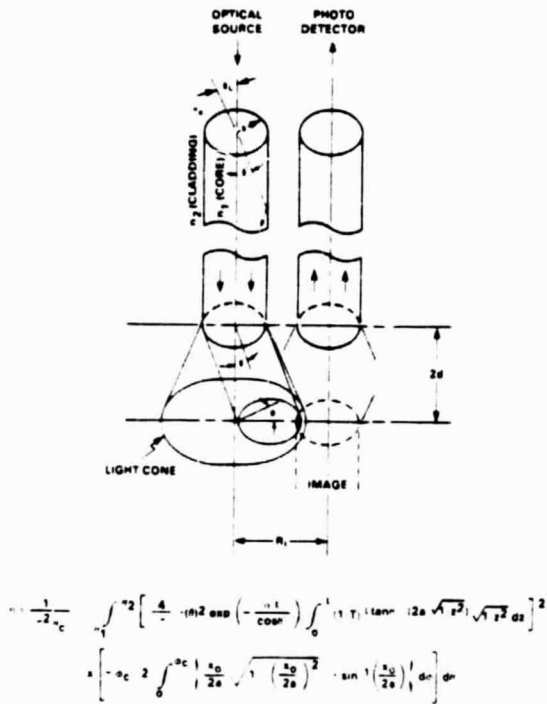


Figure 1. Geometry of two-fiber system.

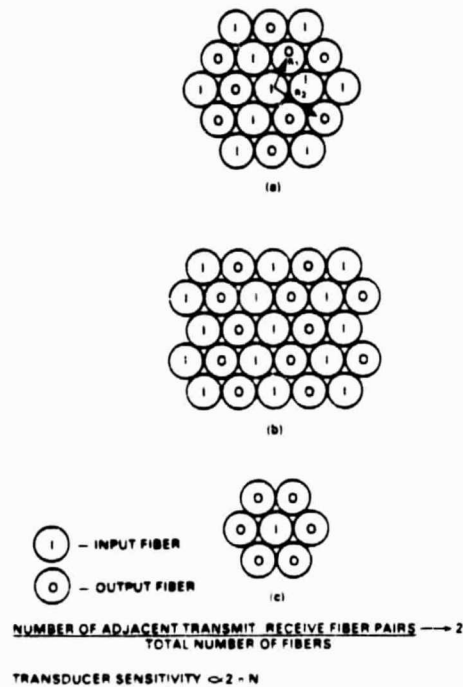
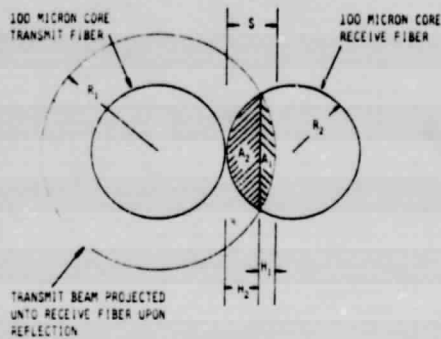


Figure 2. Fiber distribution at distal end.

ORIGINAL PAGE IS
OF POOR QUALITY



$$H_1 = \frac{S(2R_1 - S)}{2(R_1 + R_2 - S)}$$

$$H_2 = \frac{S(2R_2 - S)}{2(R_1 + R_2 - S)}$$

$$A_1 = R_1^2 \cos^{-1} \frac{H_1 - H_2}{R_1} - (R_1 - H_1) \sqrt{2R_1 H_1 - H_1^2}$$

$$A_2 = R_2^2 \cos^{-1} \frac{H_2 - H_1}{R_2} - (R_2 - H_2) \sqrt{2R_2 H_2 - H_2^2}$$

ILLUMINATED AREA OF RECEIVE FIBER = $A_1 + A_2$

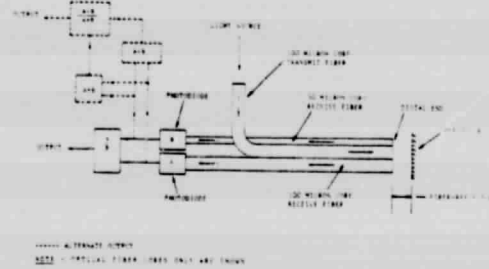


Figure 3. Method to determine illuminated areas of receive fibers.

Figure 4. A three-fiber lever transducer.

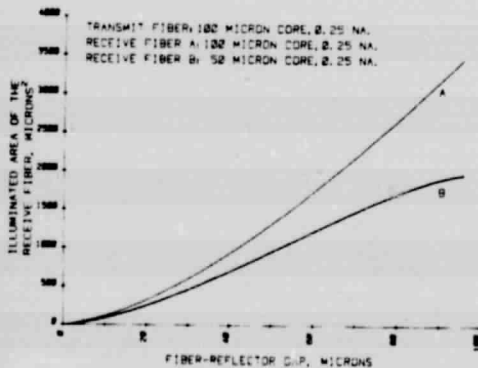


Figure 5. Illuminated areas of 100 and 50 μ receive fibers.

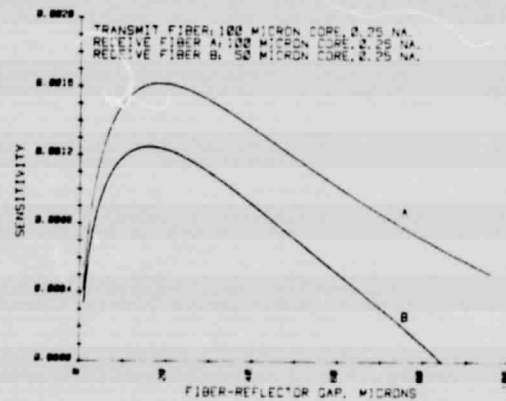


Figure 6. Sensitivity of 100/100 and 100/50 μ fiber pairs.

ORIGINAL PAGE IS
OF POOR QUALITY

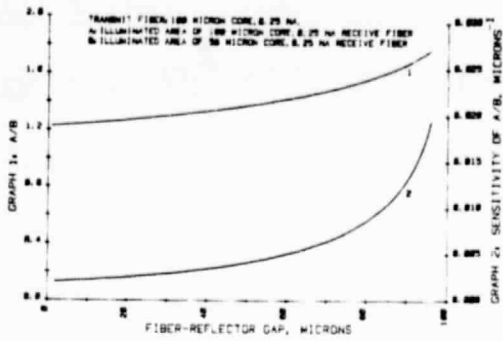


Figure 7. A/B ratio and sensitivity of 100/100/50 μm sensor.

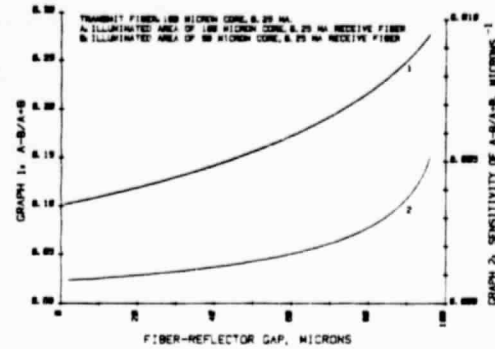


Figure 8. (A-B)/(A+B) ratio and sensitivity of 100/100/50 μm sensor.

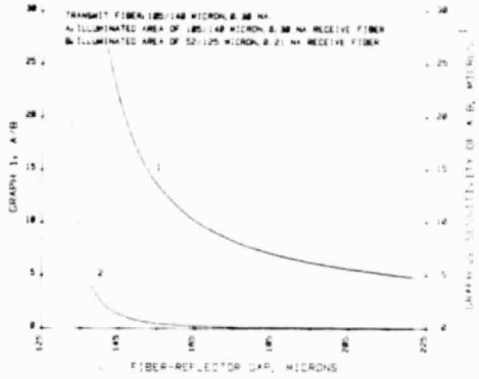


Figure 9. A/B ratio and sensitivity of 105-140/105-140/52-125 μm sensor.

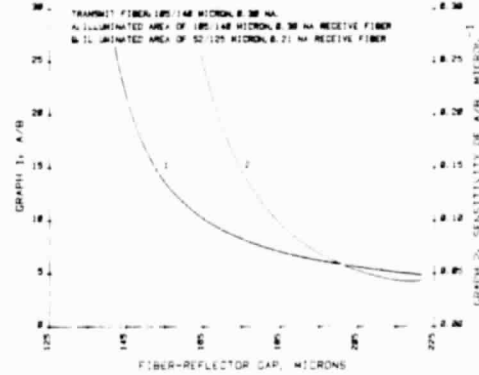


Figure 10. Data of Figure 9 with expanded sensitivity scale.

AN OPTICALLY CLEAR SILICONE RESIN AS AN ACOUSTIC ELEMENT FOR FIBER OPTIC LEVER
DISPLACEMENT SENSORS

F. W. Cuomo

Department of Physics, University of Rhode Island, Kingston, R. I. 02881 USA

One of the difficulties encountered in the design of fiber optic lever sensors is associated with the coupling of the distal end of the probe to the reflector. Since any minute dimensional change in the fiber-reflector gap requires re-calibration of the device, some method must be found to prevent, or at least minimize, this occurrence. In addition, any reflector design necessitating some form of clamping can seriously limit the frequency response of the device. In this paper, the use of optically clear elastomers is suggested to achieve an efficient sensor approach.

INTRODUCTION

The application of fiber optic levers technology has led to the development of pressure and pressure gradient hydrophones¹. More recently attention has been given to probe size reduction, improved sensitivity and extended frequency response. With suitable characteristics this type of sensor can be used for low frequency acoustic detection as well as in high frequency studies associated with acoustic imaging. The approach used by the author has been to generate a differential output from a three fiber bundle at the distal end of the lever consisting of one transmit and two receive fibers having unequal core diameters². This arrangement is shown in Figure 1. Photodiodes A and B receive the modulated light signals from the receive fiber pair and provide a divider output of much improved sensitivity. An alternate approach is also shown by dotted lines which generates an output equivalent to the difference-sum ratio. It has been found that the design criteria used at the distal end are critical to the successful operation of the device. In order to increase the bandwidth, a fiber-reflector gap relatively free of resonances requires an arrangement different from the edge-clamped diaphragm previously used. These considerations have led to the concept of an elastomeric acoustic element having suitable optical, mechanical and acoustical properties to couple the distal end of the fiber bundle to the reflector. This paper basically describes the experimental evaluation of optically clear silicone resins deemed useful for this particular application.

THEORY

A thorough analysis of the viscoelastic properties of polymers has been treated by J. D. Ferry³. In his treatise of experimental methods for bulk measurements, he defines the bulk longitudinal modulus M in its complex form

$$M^* = K^* + 4/3 G^* \quad (1)$$

where K^* is the complex bulk compression modulus and G^* the complex shear modulus. The complex nature of these quantities leads to the definitions of the storage modulus M'

$$M' = \rho v_M^2 \frac{(1-r^2)}{(1+r^2)^2} \quad (2)$$

and loss modulus M''

$$M'' = \rho v_M^2 \frac{2r}{(1+r)^2} \quad (3)$$

Similar expressions can be written for K^* and G^* . For a soft solid, in a frequency range where $G' \ll K'$, M' is practically equal to K' thus providing by bulk measurements the compressibility of the material. The quantity r in Eqns. (2) and (3) is defined as

$$r = \frac{\alpha \lambda}{2\pi} \quad (4)$$

where α is the acoustic attenuation in nepers/m and λ is the wavelength. From Eqns. (2) and (3) one also finds that for small r the loss factor $M''/M' = \tan \delta$ can be approximated by

$$\tan \delta = 2r \quad (5)$$

In simple extension the time-dependent stress $\sigma(t)$ and Young's modulus $E(t)$ are given by

$$\sigma(t) = \epsilon E(t) \quad (6)$$

where ϵ is the equivalent strain, while for a viscoelastic solid at equilibrium

$$E = \frac{9GK}{G+3K} = 2G(1+\mu) \quad (7)$$

μ being the Poisson's ratio. For soft materials with shear moduli on the order of 10^7 Pa the approach is simplified by the fact that Poisson's ratio is close to 1/2 and

$$E = 3G \quad (8)$$

EXPERIMENTAL METHODS

The evaluation of the optically clear silicone compounds under study has been performed utilizing the following techniques:

1. Static measurements
2. Dynamic measurements
 - a. Resonance methods
 - b. Ultrasonics pulse-echo methods
3. Linearity measurements

Due to space limitations the experimental data associated with parts (1), (2b) and (3) will be discussed here while part (2a), still under investigation, will be left for future treatment. Table I below lists the two-part resins along with some specifications provided by their manufacturers.

	RTV 655 (GENERAL ELECTRIC)	RTV 615 (GENERAL ELECTRIC)	SYLGARD 182 (DOW CORNING)	SYLGARD 184 (DOW CORNING)	PSW-2061 (PETRARCH SYSTEMS)	PSW-2062 (PETRARCH SYSTEMS)
SPECIFIC GRAVITY	1.03	1.02	1.05	1.05	0.98-1.01	1.00-1.06
REFRACTIVE INDEX	1.435	1.406	1.430	1.430	1.4066	1.4950
DISSIPATION FACTOR	0.001 (100 Hz)	0.001 (100 Hz)	0.001 (60 Hz)	0.001 (60 Hz)		
DIELECTRIC CONSTANT	3.00 (100 Hz)	3.00 (100 Hz)	2.70 (60 Hz)	2.75 (60 Hz)		
HARDNESS, SHORE A	50	45	40	35	18-26	8-20
WATER ABSORPTION			0.1% - 7 DAYS	0.1% - 7 DAYS		

TABLE I. CLEAR SILICONE ELASTOMERS

(a) Static measurements

The static Young's modulus was determined utilizing cylindrical samples. The results given below in Table II represent the average of elongations due to a mass increase ranging from 10 to 200 grams. The resolution is estimated to be about 10 microinches.

SAMPLE	655	615	182	184	2061	2062
YOUNG'S MODULUS ($\times 10^6$ Newtons/m ²)	2.41	1.34	1.50	2.07	0.84	0.71

TABLE II. STATIC YOUNG'S MODULI

Based on these measurements, it is possible to predict the displacement associated with a minimum acoustic pressure of 50 dB re 1 μ Pa. For the PSW-2062 sample, for instance, this pressure corresponds to a displacement of 4.45×10^{-12} m for a sample thickness of 10^{-2} meters. In addition, from eq. (7) of reference (1), the compliance can be calculated for a given sample cross-section. If a Poisson's ratio near 1/2 is assumed, a shear modulus of about 2.37×10^5 N/m² results.

(b) Dynamic measurements

Sound speed data were obtained at frequencies ranging from 0.6 to 2 MHz, both in air and water, as illustrated in Figure 2. The apparatus used for the in-air measurements is shown in Figure 3. These methods provided the information necessary to calculate the bulk longitudinal modulus M, the attenuation α and the loss factor $\tan \delta$. Table III lists the results for three of the samples tested.

SAMPLE	f, MHz	$v_M (\times 10^3$ m/s)		M ($\times 10^9$ N/m ²)	α (NEPERS/m)	τ ($\times 10^{-3}$)	$\tan \delta$ ($\times 10^{-2}$)
		IN-AIR	IN-WATER				
RTV-655	0.6	1.078		1.198	27.46	7.85	1.57
	1.0	1.076	1.075	1.193	28.89	4.95	0.99
	2.0	1.076		1.193	29.88	2.56	0.51
SYLGARD 182	0.6		1.033	1.120	23.86	6.54	1.31
	1.0		1.034	1.123	31.01	5.10	1.02
	2.0		1.034	1.122	39.52	3.25	0.65
PSW-2061	0.6	1.008		1.016	7.94	2.12	0.43
	1.0	1.008		1.015	9.01	1.45	0.29
	2.0	1.005		1.010	17.56	1.40	0.28

TABLE III. ULTRASONIC MEASUREMENTS

Measurement accuracies within $\pm 2\%$ were attained. A small decrease in sound speed is noted for a corresponding decrease in material hardness. A decrease in sound attenuation and loss factor is also observed with a decrease in hardness. Figure 4 shows typical oscilloscope traces illustrating the operation in the single pulse and tone burst modes. Immersion-type transducers (KB-Aerotech Style ISS) were used for these measurements (Fig. 3).

(c) Linearity measurements

The linear behavior of the elastomeric element when subjected to sub-micron motion is relevant to the operation of the fiber optic lever device. Efforts have been made to establish their linear characteristics within the micron displacement range. The method utilizes the dielectric properties of the silicone compounds to detect changes in capacitance as a function of displacement variations. Thus the measurement becomes associated with a capacitive-type transducer. In order to establish the resolution necessary to the detection of minute motions (1 micron or less), a quad diode bridge, whose block diagram is shown in Figure 5, is used. This signal conditioning device can be utilized for a range of 4 to 200 pF and it provides a high output with excellent linearity. To remain within the capacitance range two samples 5 cm in diameter and 1 cm thick were cemented between two electrodes, as shown in Figure 6. This arrangement provided an equilibrium capacitance of 5.38 pF

ORIGINAL PAGE IS
OF POOR QUALITY

for each sample. Figure 7 shows the test apparatus which was assembled for this work. Two Lansing differential screw translators with a resolution of one microinch ($2.54 \times 10^{-5} \text{m}$) were mounted at right angles to allow adjustment in two directions. Figure 8 gives preliminary results for the RTV-655 sample, which establish the feasibility of this type of measurement. Present efforts include the detection of sub-micron motions requiring very stable and low-noise electronics.

CONCLUSIONS

The mechanical and acoustical properties of several elastomeric compounds suitable for use as compliant elements in a fiber optic lever pressure sensor have been presented. These parameters have been experimentally determined using static and dynamic measurement methods. The results gained from this investigation suggest that the utilization of optically clear silicone resins is suitable for this application.

REFERENCES

1. Cuomo, F. W., "Pressure and pressure gradient fiber-optic lever hydrophones," J. Acoust. Soc. Am. 73(5), 1848-1857 (1983).
2. Cuomo, F. W., "The analysis of a three-fiber lever transducer," Proc. SPIE Symposium East, 478, 28-32 (1984).
3. Ferry, J. D., "Viscoelastic properties of polymers," John Wiley & Sons, Inc., New York (1980).

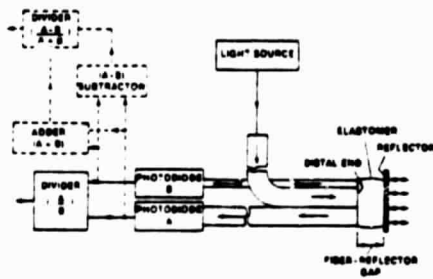


FIGURE 1

DETERMINATION OF V_{SH}



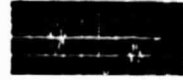
FIGURE 2



FIGURE 3



INPUT PULSE
 $T = 0.001$
 2 VOLTS/cm
 1 MHz



RTV 885
 $A_1 = 2.000 \text{ cm}$
 $A_2 = 23.875 \text{ s}$
 1 MHz
 $5.000 \text{ cm} / 2 \text{ VOLTS/cm}$



RTV 855
 $A_1 = 2.000 \text{ cm}$
 $A_2 = 23.875 \text{ s}$
 1 MHz
 $10.000 \text{ cm} / 1 \text{ VOLT/cm}$

FIGURE 4

CIRCUIT BLOCK DIAGRAM

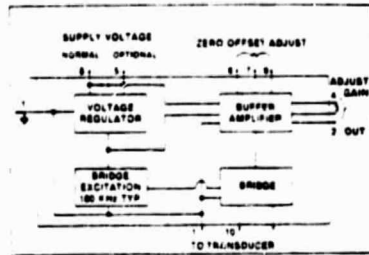


FIGURE 5

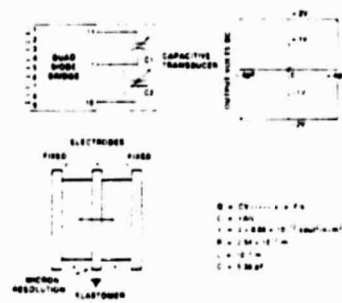


FIGURE 6



FIGURE 7

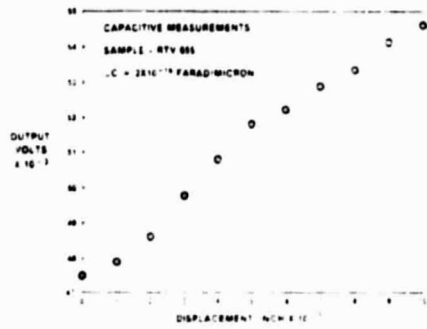


FIGURE 8

A FIBER OPTIC LEVER SENSITIVE TO SHEAR STRESS

Robert S. Kidwell

Department of Physics, University of Rhode Island, Kingston, RI 02881
and

Frank W. Cuomo

Department of Physics, University of Rhode Island, Kingston, RI 02881
and

Naval Underwater Systems Center, Newport, RI 02841

ABSTRACT

A fiber optic lever sensing technique that can be used to measure shear stresses is discussed. This technique uses three unequal fibers, combining small size and high sensitivity. Experimental data appear to confirm theoretical model predicted by geometrical optics.

INTRODUCTION

Non-contacting fiber optic levers have been described for a range of applications including pressure transducers, pressure and pressure gradient hydrophones and shock measurements^{1,2,3,4}. Lawson and Tekippe⁴ measured pressure using diaphragm curvature. Their method related diaphragm curvature to the ratio of light intensity received by two sets of fibers concentric with the source fibers. Using the ratio of received intensity compensates for input power variations, as well as fiber and coupling losses. All fibers were of equal core diameters. McMahon et al⁵ describe a hydrophone based on the photoelastic effect, which also uses an output ratio method. Cuomo⁶ describes a technique, which uses only three fibers, one transmit and two receive, of unequal core dimensions. Light is reflected from a diaphragm and is collected by the two receive fibers, with the ratio of their outputs determining the sensitivity. He uses a geometric determination of the illuminated areas of the receive fibers to predict sensitivities as a function of fiber-reflector gap. Use of unequal receive fiber core diameters results in improved sensitivities which permit the consideration of such a small number of fibers in the sensor.

This paper describes a related method which uses the same three fiber arrangement, but is sensitive to shear stress rather than pressure. While other sensors have used a diaphragm undergoing normal motion relative to the fiber ends, shear motion can be detected by employing a floating element reflective only on half the area illuminated by the transmit fiber. Motion parallel to the fiber ends is then translated directly into modulation of the output light intensity of the receive fibers. A geometrical optics method is used to predict sensitivities. Our data indicate the feasibility of a sensor of this type.

THEORY

It has been shown⁶ that it is possible using geometrical optics to obtain an approximation to device sensitivity for the case of a reflector whose motion is normal to the fiber ends. Similarly, sensitivities can be approximated for reflector motion parallel to the fiber ends. In either case it is unnecessary to consider optical fiber losses, reflectivity losses and similar factors. Figure 1 shows the cross-section of three adjacent step-index fibers. Fiber specifications are given in Table 1.

TABLE I

Fiber	Core Diameter (microns)	Cladding Diameter (microns)	Numerical Aperture
Transmit	200	240	0.30
Receive (A)	200	240	0.30
Receive (B)	52	125	0.21

Reflected back on the plane of the fiber surfaces is the area of illumination due to the transmit fiber. This area varies with the fiber-reflector distance but for a sufficiently large distance a fully reflecting element would completely illuminate both receive fibers as shown. Only part of the illuminated region of the reflector is reflective. A straight line marks the edge of the reflective portion. The remaining portion of the reflector is assumed non-reflective, with the result that the illuminated areas on the receive fibers depend on the parallel reflector displacement. The figure shows the resulting illuminated areas A and B of the large and small receive fibers and the total area of illumination due to the transmit fiber. Since the irradiance is radiant flux per unit area, one can write

$$\begin{aligned} P_A/P_O &= A/S \\ P_B/P_O &= B/S \end{aligned} \tag{1}$$

where P_A , P_B and P_O are the radiant flux in watts, at the plane of Figure 1, for the receive fibers and the transmit fiber, respectively, and S is the area of illumination due to the transmit fiber. With a single receive fiber a small reflector displacement dq lead to a small change in A/S such that the sensitivity becomes

$$d(A/S)/dq. \tag{2}$$

One can instead take the ratio of equations (1) for the case of two different receive fibers, and obtain

$$\frac{P_A/P_O}{P_B/P_O} = \frac{A/S}{B/S} = \frac{A}{B} \tag{3}$$

Note that by taking the ratio the term S is eliminated. The ratio sensitivity is thus simply

$$d(A/B)/dq \tag{4}$$

For simplicity Figure 1 illustrates three fibers of equal numerical aperture, but the model easily accomodates different numerical apertures for the three fibers. This model can be used to determine optimum choices of transmit and receive fiber core and cladding diameters, the distance between fiber centers and numerical apertures.

Data were generated using this model, with the fiber parameters given in Table 1. Figure 2 shows the illuminated areas of the receive fibers as a function of reflector displacement. The reflector displacement is referenced to the center line of the transmit fiber. Figure 3 shows the ratio sensitivity. The model predicts remarkably high values for sensitivity. In addition, the optimum fiber to reflector distance is quite large, making design requirements less exacting.

EXPERIMENTAL METHODS

To test the model a prototype sensor was constructed. The design is shown in Figure 4. Three commercially available step-index glass fibers were assembled in a short metal sheath. An ultrathin front surface mirror was used as the reflector, with the mirror edge providing the reflective to non-reflective edge. The light source was a Motorola MFOE1201 LED with a peak wavelength

ORIGINAL PAGE IS
OF POOR QUALITY

of 820 nm, and two UDT FO-02 400 photodiodes were used for detection. The source was voltage modulated with a square wave and the photodiode outputs filtered (1 Hz band) through lock-in amplifiers. For these tests the output ratio was calculated from separate output signals. Mirror displacements parallel to the fiber end were made using a micrometer having a resolution of .025 microns in order to establish the sensor operation as a shear sensor and also to confirm the theory shown in Figures 2 and 3. The fiber-reflector gap was chosen to maximize the total light throughput. Figures 5 and 6 show the results of the tests. Output power from the detector for both receive fibers are plotted against mirror displacement in Figure 5, while Figure 6 shows the sensitivity $d(A/B)$ versus displacement.

CONCLUSIONS

It has been shown as indicated by comparison of Figures 2, 3 and 5, 6 that the simple model used here effectively predicts sensor behavior. The experimental data in Figure 6 shows high values of sensitivity in agreement with the model.

The arrangement of fibers described here provides the potential of building small devices for detecting shear stresses, as well as extension to other applications in acoustic detectors, flow measurements and other areas. It has been shown that geometrical optics, using the illuminated areas method, can be used to predict sensitivities and operating ranges for fiber optic lever sensors. This technique can be effectively used to optimize such fiber parameters as core and cladding dimensions, spacing between fibers and relative orientation.

ACKNOWLEDGEMENT

This work was supported by the National Aeronautics and Space Administration through Grant #NAG1-519.

REFERENCES

1. K. Kobayashi, H. Okuyama, T. Kato and T. Yasuda, "Fiberoptic catheter-tip micromanometer," *J.J. Med. Electron, Biol. Eng.* 15, 25-32 (1977).
2. R.O. Cook, C.W. Hamm and A. Akay, "Shock measurement with non-contacting fiber optic levers," *J. Sound Vib.* 76, 443-456 (1981).
3. F.W. Cuomo, "Pressure and pressure gradient fiber optic lever hydrophones," *J. Acoust. Soc. Am.* 73, 1848-1857 (1983).
4. C. Lawson and V.J. Tekippe, "Fiber-optic diaphragm-curvature pressure transducer," *Opt. Lett.* 8, 286-288 (1983).
5. D.H. McMahon, R.A. Soref and L.E. Sheppard, "Sensitive fieldable photoelastic fiber-optic hydrophone," *J. Lightwave Technol.* LT-2, 469-478 (1984).
6. F.W. Cuomo, "The analysis of a three-fiber lever transducer," *Proceedings of the SPIE Technical Symposium*, 478, 28-32 (1984).

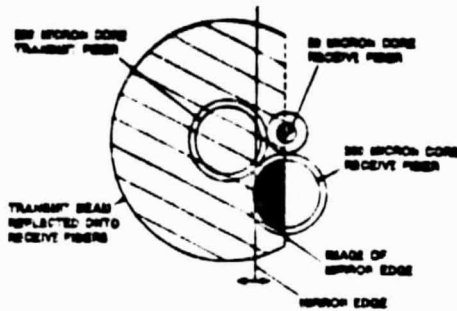


Figure 1. Distribution of transmit and receive fibers.



Figure 2. Illuminated areas of 200 and 50 micron receive fibers.

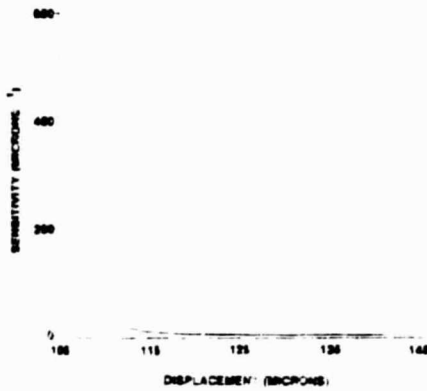


Figure 3. Sensitivity of three-fiber sensor.

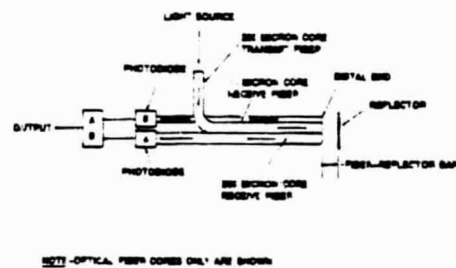


Figure 4. A three-fiber lever transducer.

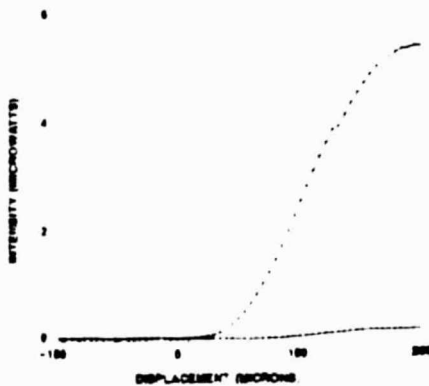


Figure 5. Intensity output of receive fibers (experimental).
 \times - 200 μ m fiber. \circ - 50 μ m fiber.

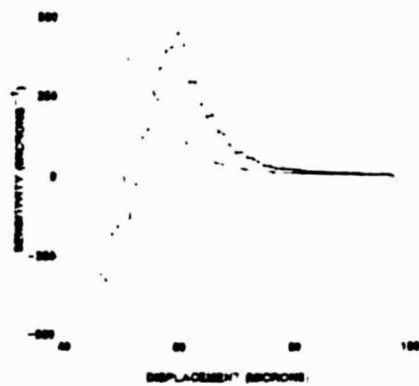


Figure 6. Sensitivity of transducer (experimental).
 \times - 5 μ m intervals \circ - 1 μ m intervals.

SUMMARY REPORT I

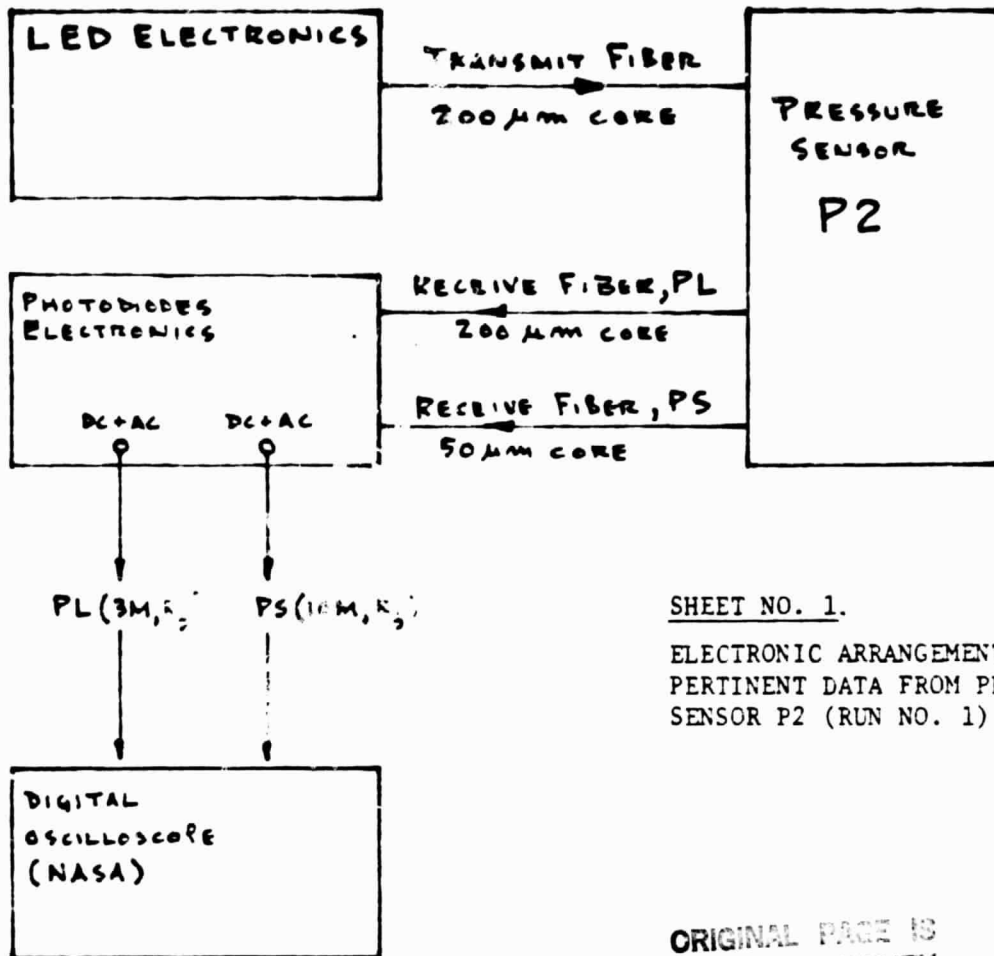
Langley Research Center Wind Tunnel Experiment

This is a summary of the data pertaining to our recent wind tunnel experiments at Langley Research Center. Basically two runs were made.

Run no. 1 was done according to sheets nos. 1 and 2. Pressure sensor P2 and shear sensor S2 were used for all measurements and were assembled according to Figures 1 and 2. Please note that measurements for this run were taken only at zero flow and at 122 Ft/s wind tunnel speed. During this run the output from the photodiode electronics contained both DC and AC information and Ralph was able to obtain data in the DC and AC coupled modes, as indicated.

Run no. 2 was performed according to sheets nos. 3 and 4. During this run AC measurements were made at several wind speeds and the results are summarized in Graph no. 1. It is worthy to note that above 60 Ft/s speeds a positive response from the 200 micron fiber was evident. It is also of interest that for both the shear and pressure sensors a peak in outputs is observed at about 100 Ft/s. Hopefully, Ralph may be able to explain this. It should be indicated that all AC measurements in run no. 2 were taken using the PAR pre-amplifier. The increase in gain compared to the data of run no. 1 was 200 to 1. The actual signals recorded provided 166 to 1 increase for the optical fiber PL and a corresponding 169 to 1 increase for the optical fiber SL. The discrepancies can be associated with the inclusion of a 3 Hz/3kHz bandwidth.

We wish to indicate that, due to the poor performance of the 50 micron fiber, we were not allowed to determine the output ratio, as originally planned. I am confident that had we been able to do so the overall sensitivity would have been much better. We must realize that our measurements were made with a single receive fiber which is by far the worst case. Thus, future efforts will definitely improve the overall performance of these sensors to meet the requirements of the low speed wind tunnel and hopefully exceed them.



SHEET NO. 1.

ELECTRONIC ARRANGEMENT AND PERTINENT DATA FROM PRESSURE SENSOR P2 (RUN NO. 1)

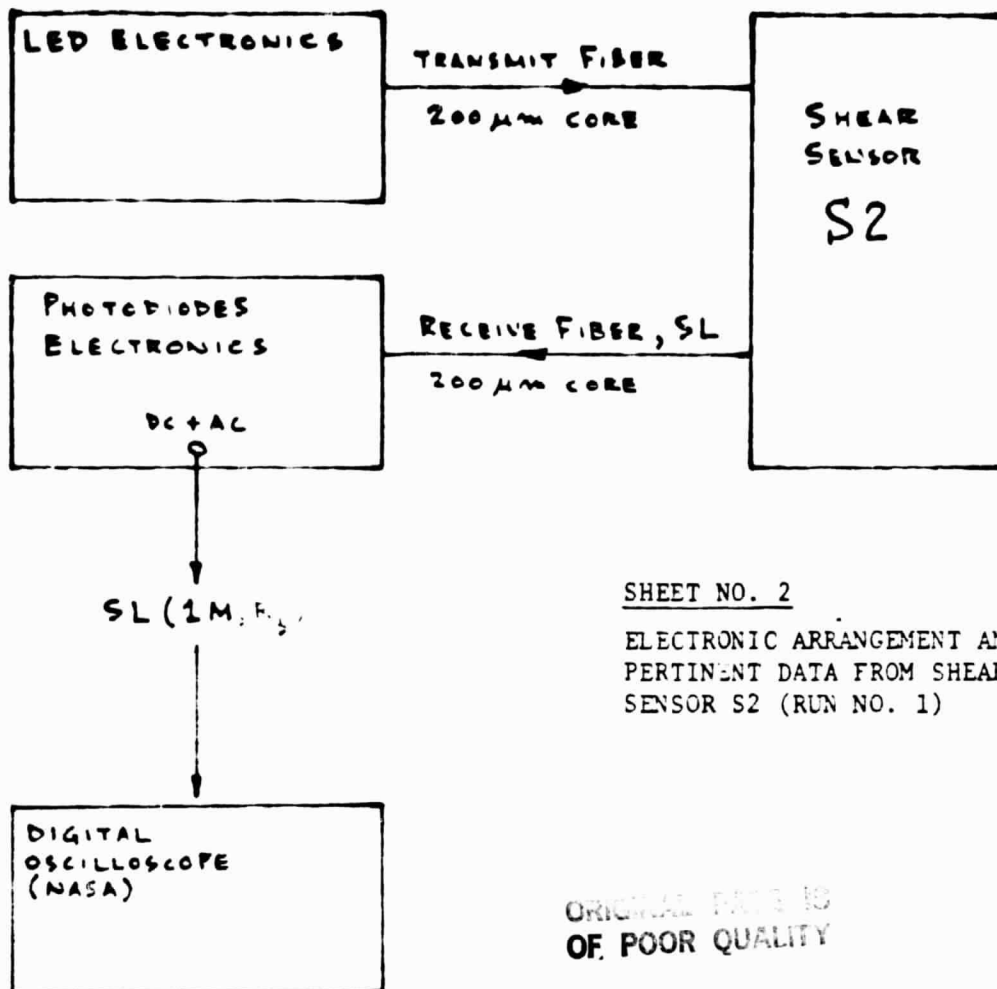
ORIGINAL PAGE IS OF POOR QUALITY

DATA (8/15/85)

	<u>PL</u>		<u>PS</u>	
	<u>DC COUPLED</u>	<u>AC COUPLED</u>	<u>DC COUPLED</u>	<u>AC COUPLED</u>
NO FLOW	-2.823 V (DC) OFFSET	890 μV (RMS)	-0.437 V (DC) OFFSET	281 μV (RMS)
122 Ft/s	-2.844 V	906 μV	-0.441 V	330 μV

NOTE: BODY OF PRESSURE SENSOR P2 WAS ASSEMBLED AT LARC ACCORDING TO FIGURE 1.

FWC 8/21/85



SHEET NO. 2

ELECTRONIC ARRANGEMENT AND
PERTINENT DATA FROM SHEAR
SENSOR S2 (RUN NO. 1)

ORIGINAL DATA IS
OF POOR QUALITY

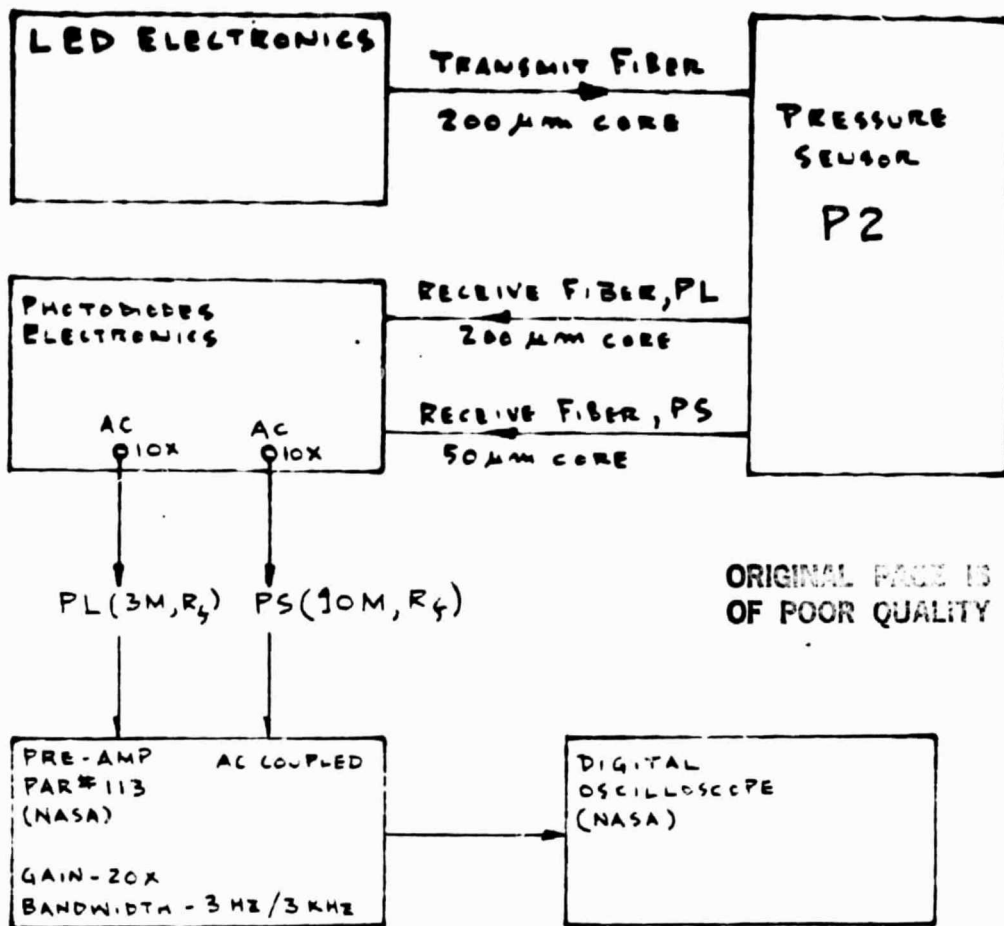
DATA (8/15/85)

	<u>SL</u>	
	<u>DC COUPLED</u>	<u>AC COUPLED</u>
NO FLOW	- 1.313 V (DC) OFFSET	171 μV RMS
122 FT/S	- 1.320 V	183 μV

NOTES: 1) RESPONSE FROM 50 μm FIBER UNCHANGED.

2) BODY OF SHEAR SENSOR S2 WAS ASSEMBLED
AT URI ACCORDING TO FIGURE 2.

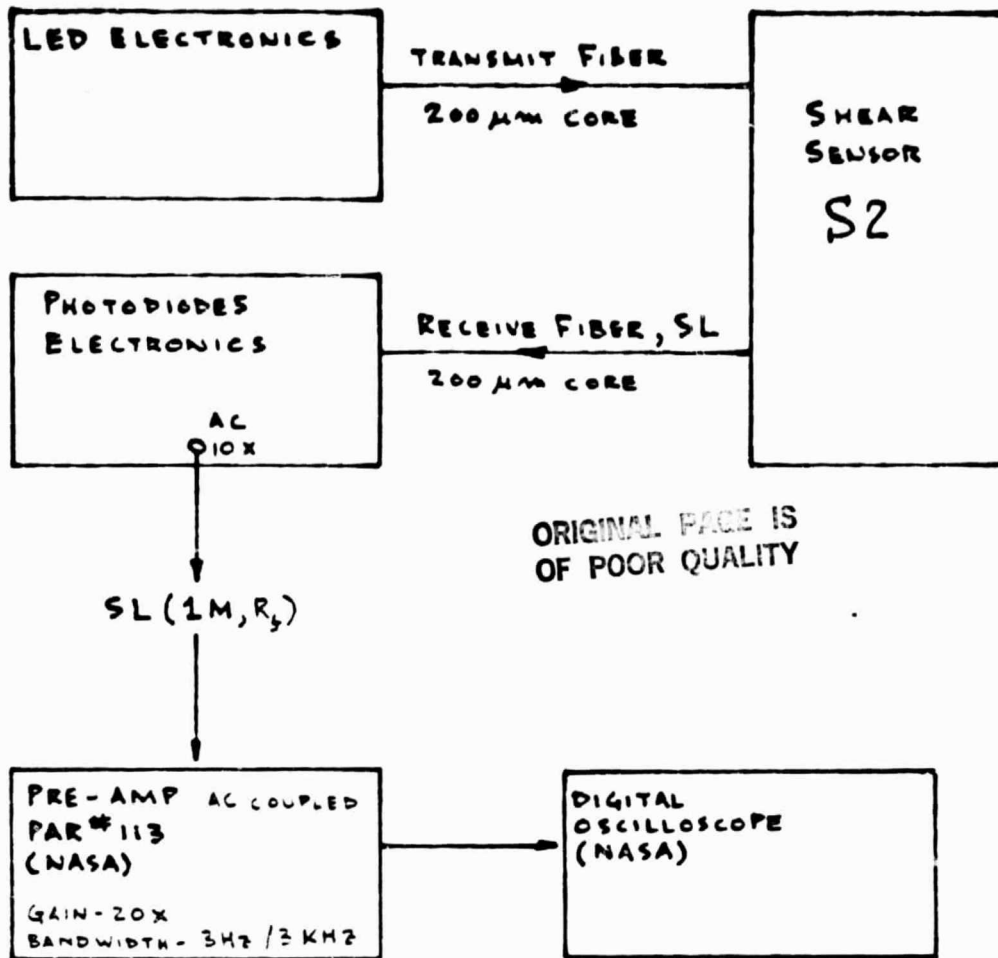
FWC 8/21/85



SHEET NO. 3

ELECTRONIC ARRANGEMENT FOR
PRESSURE SENSOR P2 (RUN NO. 2)

DATA SHOWN ON GRAPH NO. 1



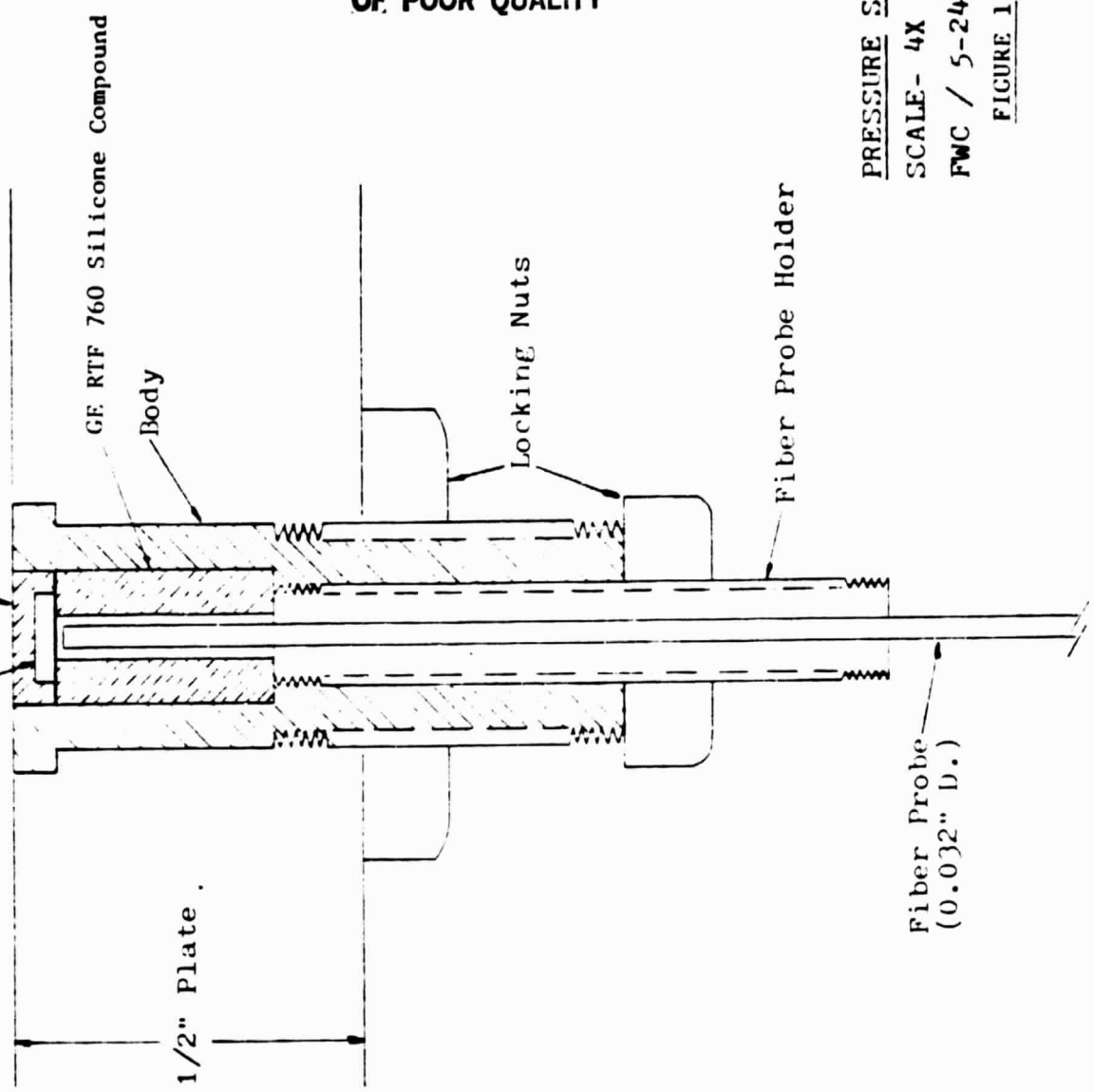
SHEET NO. 4

ELECTRONIC ARRANGEMENT
FOR SHEAR SENSOR S2
(RUN NO. 2)

DATA SHOWN ON GRAPH NO. 1

Reflector
(Dimensions and Location
are approximate)

Elastomer, 1/16" Thick Silastic Foam Rubber



GE RTF 760 Silicone Compound

Body

Locking Nuts

Fiber Probe Holder

Fiber Probe
(0.032" D.)

1/2" Plate

ORIGINAL PAGE IS
OF POOR QUALITY

PRESSURE SENSOR P2

SCALE - 4X

FWC / 5-24-85

FIGURE 1

ORIGINAL PAGE IS
OF POOR QUALITY

Elastomer, 1/32" Petrarch Systems
PSW-2061 Silicone Rubber

Reflector
(Dimensions
approximate)

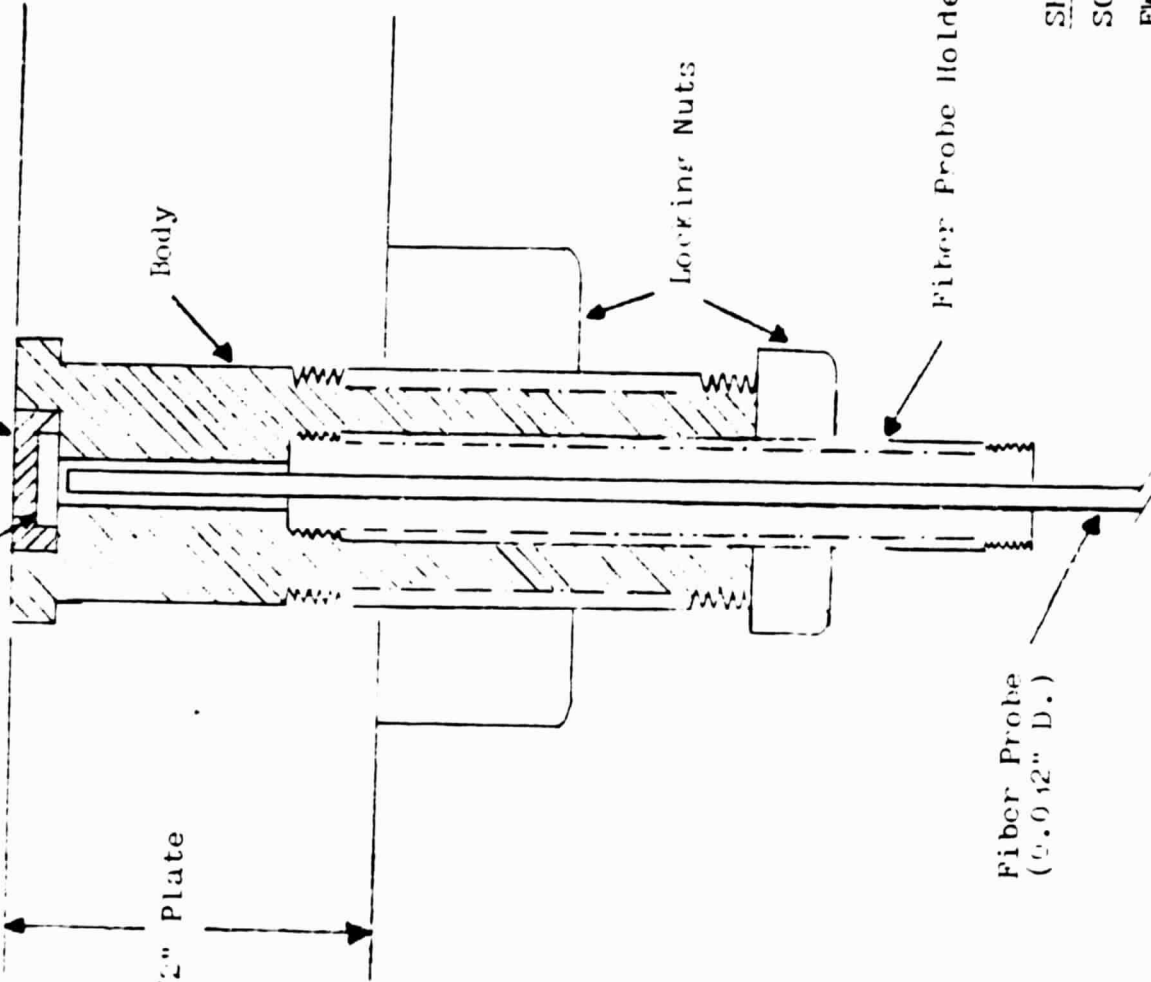
Body

Locking Nuts

Fiber Probe Holder

Fiber Probe
(0.012" D.)

1/2" Plate



SHEAR STRESS SENSOR S2

SCALE - 4X

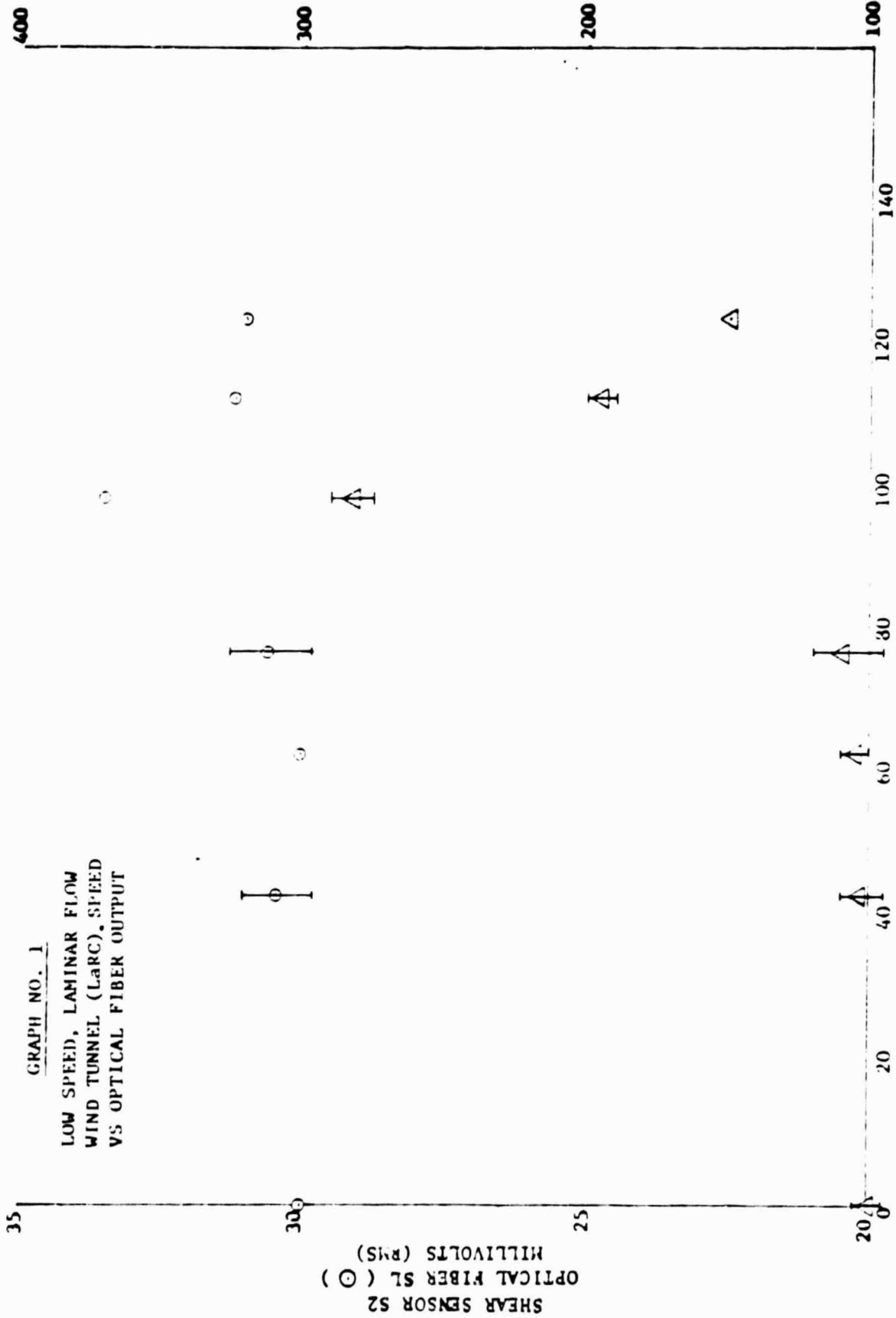
FWC-RSK / 5-30-85

FIGURE 2

NOTE: OUTPUT FROM OPTICAL FIBER PS UNCHANGED AT 531 MICROVOLTS

GRAPH NO. 1

LOW SPEED, LAMINAR FLOW
WIND TUNNEL (LaRC) SPEED
VS OPTICAL FIBER OUTPUT



FWC-8/26/85

WIND TUNNEL SPEED, FT/S

SUMMARY REPORT II

STATIC PRESSURE TEST

The purpose of this test was to characterize the magnitude and linearity of response of the 3-fiber pressure sensors to pressures somewhat above acoustic pressure levels.

Figure 1 is a diagram of the test apparatus. The sensor is mounted flush in the base of a small pressure chamber. Pressurized gas is admitted through a valve to provide static pressures to .36 psi. Pressures are determined using a magnehelic differential pressure gauge measuring in units of inches of water.

The LED light source for the fiber-optic sensor is modulated with a 2kHz square wave to provide a frequency for lock-in amplifiers. The signals from the large and small receive fibers are amplified, filtered through Ithaco lock-in amplifiers and read on digital voltmeters.

Four sensors were tested using the procedure outlined above. Sensor P1 was constructed using the elastomer G.E. RTV 602 to support the mirror and silastic foam rubber above the mirror. P2 has foamed RTF760 supporting the mirror and silastic foam rubber above the mirror. The bodies of sensors P1 and P2 were assembled at Langley by Sam Harper. Sensor P3 has Petrarch Systems elastomer 2061 both above and below the mirror while P4 has 2061 to support the mirror and 2062 above the mirror.

Figures 2 and 3 show the change in output voltage of the large and small fibers, respectively, as a function of pressure. The largest response is due to P2 which has the largest compliance. Similarly, P3 with the lowest compliance, exhibits the smallest response. Sensors P1 and P4 are similar in construction and show comparable response. In addition all of the curves show a linear response throughout the range of pressure tested.

The magnitude of change in fiber output depends not only on pressure but on the base output of the fiber, which is a function of LED power level and

coupling losses in the fiber optic system. The sensitivity of a sensor with one receive fiber is usually given as $S = (\Delta I/I) \cdot (1/\Delta p)$ where I and ΔI are the output power and output power change, respectively, and Δp is the change in pressure. Table 1 gives the sensitivities per psi for the large and small fibers individually for each sensor. In addition, the importance of a 3-fiber sensor such as these is that the change in the ratio of outputs of the large and small fibers should give an improved sensitivity over either individual fiber. Table 1 also lists the ratio sensitivity $S_R = \Delta(A/B) \cdot (1/\Delta p)$ where A is the large fiber output and B is the small fiber output. Three out of the four show significant improvement in sensitivity by using the ratio sensitivity. It should be noted that the optimum position of the fiber relative to the mirror for ratio sensitivity is not the same as the optimum for individual fiber sensitivities. These tests were conducted with the sensors adjusted for optimum individual sensitivities. Larger improvements due to using the ratio can be expected if the sensors are optimized for ratio sensitivity.

It can be seen then from the results of this test that a measurable response to pressure is obtained with all of the four sensors tested in the pressure range used. Also the sensors exhibit linearity of response over this range. Improvement of sensitivity can be achieved by using the ratio of fiber outputs rather than the individual outputs.

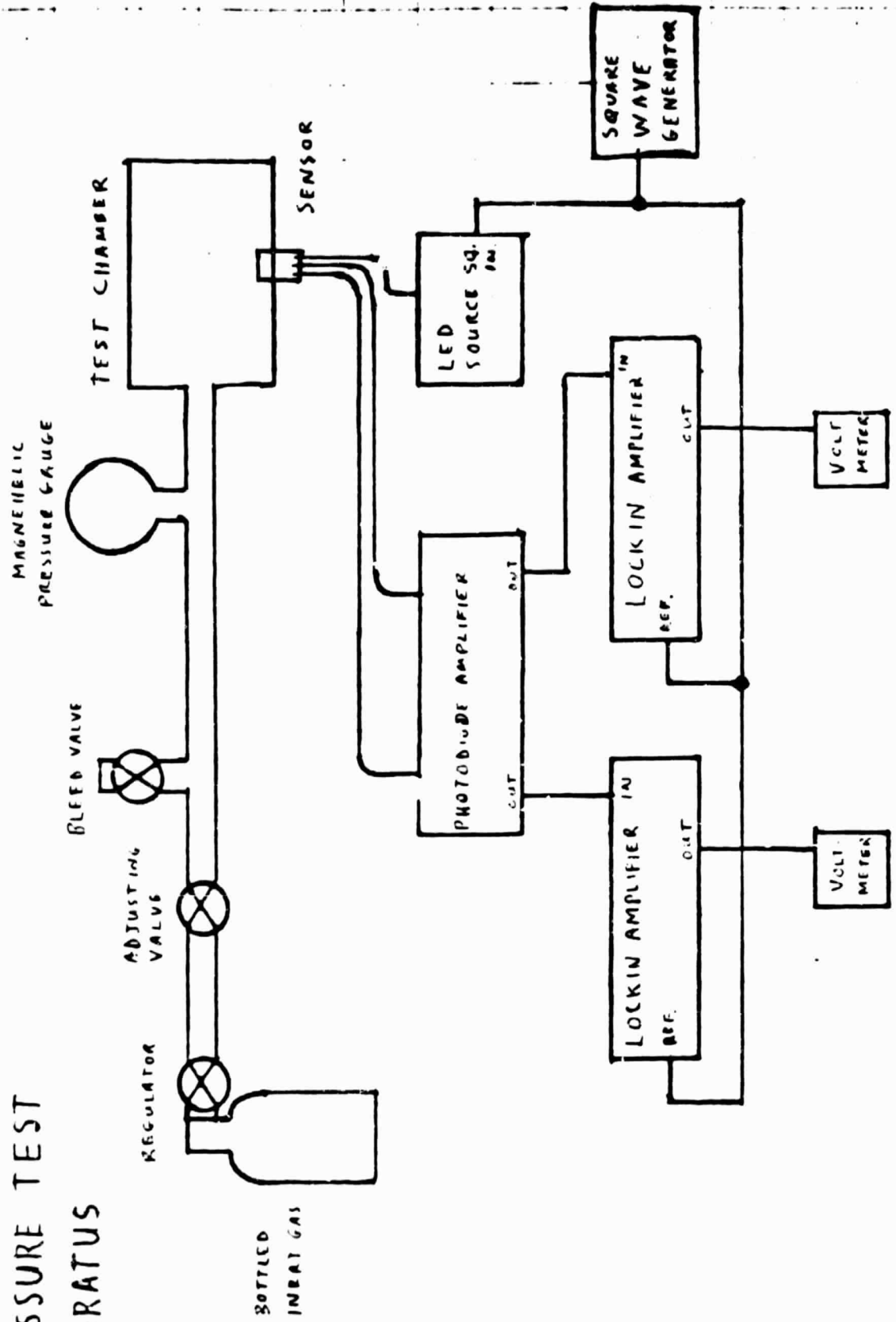
Sensitivity (psi^{-1})

Sensor	Large Fiber	Small Fiber	Ratio (Large/Small)
P1	.0314	.0243	.0731
P2	.146	.0783	.774
P3	.0543	.0136	.144
P4	.0587	.0643	.0421

TABLE 1: Sensitivity per psi for 4 probes

FIGURE 1

PRESSURE TEST APPARATUS



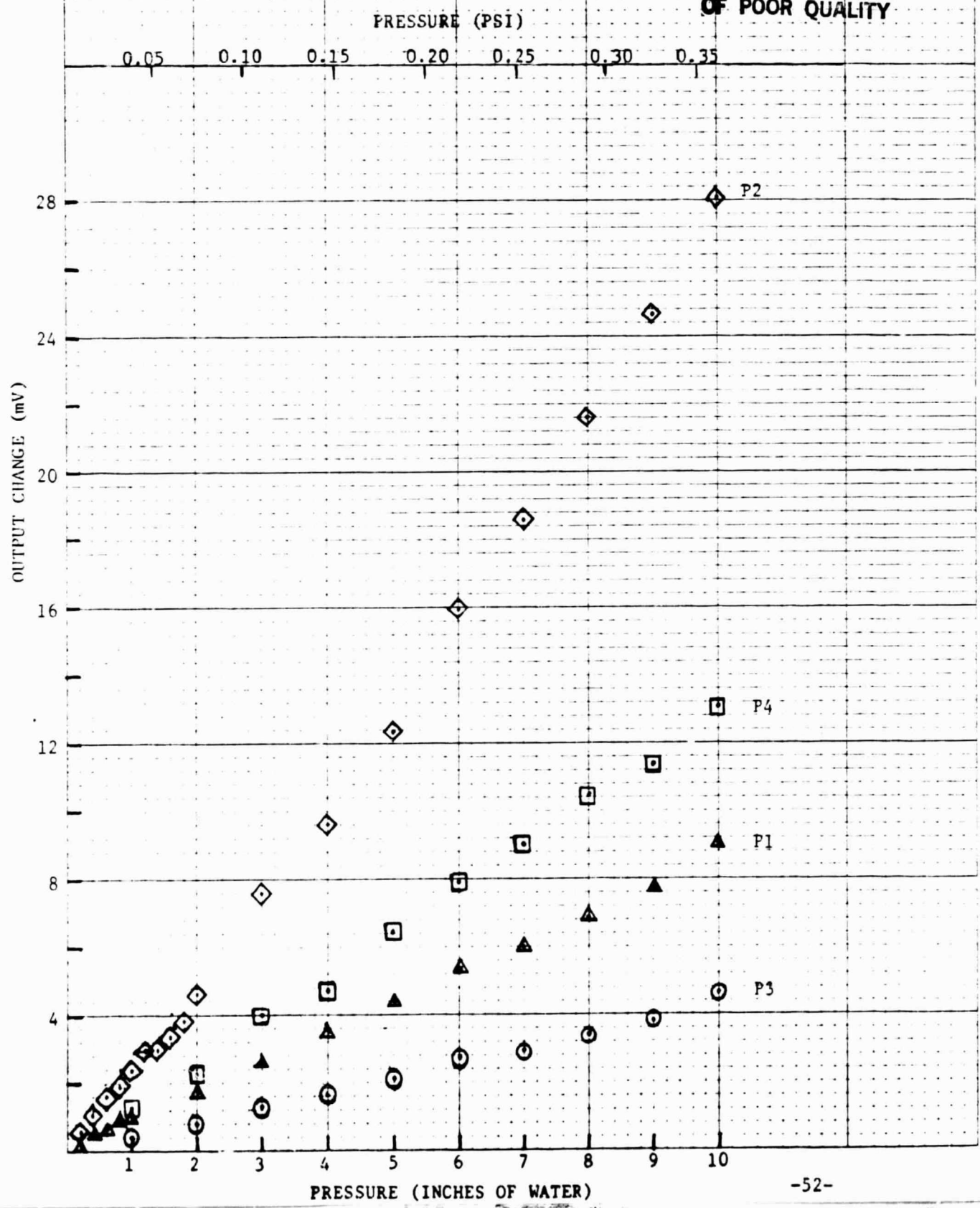
RSK

46 0700

M-2 10 X 10 TO THE INCH KEUFEL & ESSER CO. MADE IN U.S.A.

FIGURE 2
CHANGE IN OUTPUT OF LARGE FIBER VS. PRESSURE

ORIGINAL PAGE IS
OF POOR QUALITY



46 0700

FIG. 3 MAX. 10 TO THE INCH.
KIMBLE & BENDIS CO. 1954

FIGURE 3
CHANGE IN OUTPUT OF SMALL FIBER VS. PRESSURE

ORIGINAL PAGE IS
OF POOR QUALITY

